Journal of Vertebrate Paleontology

ISSN: 0272-4634 (Print) 1937-2809 (Online) Journal homepage: http://www.tandfonline.com/loi/ujvp20

New material of a 'short-faced' Trogosus (Mammalia, Tillodontia) from the Delmar Formation (Bridgerian), San Diego County, California, U.S.A.

Kazunori Miyata & Thomas A. Deméré

To cite this article: Kazunori Miyata & Thomas A. Deméré (2016) New material of a 'short-faced' Trogosus (Mammalia, Tillodontia) from the Delmar Formation (Bridgerian), San Diego County, California, U.S.A., Journal of Vertebrate Paleontology, 36:3, e1089878, DOI: 10.1080/02724634.2016.1089878

To link to this article: http://dx.doi.org/10.1080/02724634.2016.1089878

Journal of Vertebrate Paleontology e1089878 (27 pages)

DOI: 10.1080/02724634.2016.1089878

ARTICLE

NEW MATERIAL OF A 'SHORT-FACED' *TROGOSUS* (MAMMALIA, TILLODONTIA) FROM THE DELMAR FORMATION (BRIDGERIAN), SAN DIEGO COUNTY, CALIFORNIA, U.S.A.

KAZUNORI MIYATA*[,1,2] and THOMAS A. DEMÉRÉ[3]
[1]Institute of Dinosaur Research, Fukui Prefectural University, 4-1-1 Kenjojima, Matsuoka, Eiheiji-Town, Fukui 910-1195, Japan;
[2]Fukui Prefectural Dinosaur Museum, 51–11 Terao, Muroko, Katsuyama City, Fukui 911–8601, Japan,
k-miyata@dinosaur.pref.fukui.jp;
[3]Department of Paleontology, San Diego Natural History Museum, P.O. Box 121390, San Diego, California 92112–1390, U.S.A.,
tdemere@sdnhm.org

ABSTRACT—The 'Swami's Point local fauna,' recovered from the Delmar Formation in coastal San Diego County, California, U.S.A., represents the first documented Bridgerian vertebrate assemblage in this region. The Delmar Formation is chronologically constrained (ca. 48–47 Ma) on the basis of paleomagnetic polarities, the superposition of marine strata containing nannofossils of the CP 12b subzone, and occurrences of the Bridgerian index taxa *Trogosus castoriden*s and *Hyrachyus modestus*. The specimen of *Trogosus* (SDSNH 40819) is assigned here to the genotypic species, *T. castoridens*, hitherto known only from incomplete dentaries from the middle Bridgerian (Br2) Bridger Formation, Green River Basin, Wyoming. The present specimen is represented by a skull with diagnostically short rostrum, incomplete stylohyoids, posterior parts of both dentaries, and cervical vertebrae from a single individual. This is one of the most anatomically informative specimens of *Trogosus* and for the first time provides details of the basicranial region in the order Tillodontia. A well-preserved occipitomastoid process is clearly composed of the mastoid process of the petrosal and the paracondylar process of the exoccipital. Cranial comparison reveals greater similarity with *T. hyracoides* from the Bridger Formation than with *T. grangeri* and *T. hillsii* from the Huerfano Basin, Colorado. The results of a phylogenetic analysis suggest that the short-faced condition evolved at least twice in species of *Trogosus* and leads to recognition of two sympatric trogosine species pairs: *T. hyracoides* + *T. castoridens* from the Green River Basin and *T. grangeri* + *T. hillsii* from from the Huerfano Basin.

SUPPLEMENTAL DATA—Supplemental materials are available for this article for free at www.tandfonline.com/UJVP

Citation for this article: Miyata, K., and T. A. Deméré. 2016. New material of a 'short-faced' *Trogosus* (Mammalia, Tillodontia) from the Delmar Formation (Bridgerian), San Diego County, California, U.S.A. Journal of Vertebrate Paleontology. DOI: 10.1080/02724634.2016.1089878.

INTRODUCTION

The only known vertebrate fossils of Bridgerian age from California have been recovered from the Delmar Formation in coastal San Diego County (Walsh, 1996; Robinson et al., 2004) and comprise a low-diversity assemblage of reptiles and mammals. This assemblage was named the "Swami's Point local fauna" by Walsh (1996:77) and includes a crocodilian, *Pristichampsus* sp., a basal rhinocerotoid, *Hyrachyus* sp. (= *H. modestus* in this paper), and a trogosine tillodont, *Trogosus* sp. (= *T. castoridens* in this paper). Despite the paucity of material, this local fauna is significant, because the combination of *Trogosus* and *Hyrachyus* indicates a correlation with the Bridgerian North American Land Mammal Age (NALMA) (Robinson et al., 2004; Woodburne, 2004; Gunnell et al., 2009). Vertebrate fossil remains from other localities in the Delmar Formation consist of unidentified, fragmentary remains of bony fishes, turtles, crocodiles, and rodents (Walsh, 1996). The specimens of *Trogosus* and *Hyrachyus* from the Delmar Formation remained undescribed and unprepared until recently, although the former includes a nearly complete, informative skull with well-preserved basicranium, SDSNH 40819. This specimen represents the only diagnostic tillodont material from the western United States.

This paper focuses on the taxonomy of *Trogosus* from the Delmar Formation through comparisons with other trogosine species and comments on the phylogeny of North American *Trogosus*. The Delmar Formation *Hyrachyus* specimen (SDSNH 55276) is also briefly described and illustrated for the first time.

Trogosus, the type genus of the Trogosinae Gazin, 1953, is the best-known and anatomically most well-documented tillodont genus. *Trogosus* has been recorded from earliest to middle Bridgerian (Br1a–Br2; Gardnerbuttean–late Blacksforkian) in the Western Interior of the United States, mostly from Wyoming and Colorado (Gunnell, 1998; Robinson et al., 2004; Miyata, 2007a, 2007b; Gunnell et al., 2009). As discussed below, the Delmar Formation *Trogosus* can be referred to the type species, *T. castoridens* Leidy, 1871, which previously was known only from the holotype, ANSP 10337, an incomplete partial mandible consisting of right and left dentaries and a damaged lower dentition. Currently, there are five other valid species of *Trogosus*, including *T. hyracoides* (Marsh, 1873), *T. latidens* (Marsh, 1874), *T. grangeri* Gazin, 1953, *T. hillsii* Gazin, 1953, and *T. gazini* Miyata, 2007b (Gazin, 1953, 1976; Stucky and Krishtalka, 1983; Miyata, 2007a, 2007b). A more robust North American trogosine, *Tillodon fodiens* Gazin, 1953, is the sole member of the monotypic genus *Tillodon*, known from Br2 strata in Wyoming. This species is considered to belong to or to be closely related to the genus *Trogosus* (Lucas and Schoch, 1998; Miyata, 2007b). In addition, a few close relatives of *Trogosus* have been described outside

*Corresponding author.

North America, based on incomplete fossil material from the middle Eocene of China (*Kuanchuanius shantungensis* Chow, 1963) and Japan (cf. *Trogosus* sp., *Trogosus* cf. *T. latidens*; see Miyata and Tomida, 1998; Miyata, 2007a).

Abbreviations, Materials, and Terminology

Institutional Abbreviations and Comparative Materials—**AMNH**, American Museum of Natural History, New York, New York, U.S.A.; **ANSP**, Academy of Natural Sciences of Philadelphia, Pennsylvania, U.S.A.; **FPDM**, Fukui Prefectural Dinosaur Museum, Katsuyama, Fukui, Japan; **SDSNH**, San Diego Natural History Museum, San Diego, California, U.S.A.; **UM**, University of Michigan, Museum of Paleontology, Ann Arbor, Michigan, U.S.A.; **USNM**, United States National Museum of Natural History, Washington, D.C., U.S.A.; **YPM**, Peabody Museum of Natural History, Yale University, New Haven, Connecticut, U.S.A.

Unless otherwise noted, the descriptions given below are based on skeletal elements of the Delmar Formation specimen, SDSNH 40819. Comparisons of cranial morphology with other specimens of *Trogosus* were made on the basis of USNM 17886 (*T. hyracoides*), AMNH 17008 (*T. grangeri*, holotype), and USNM 17175 (*T. hillsii*, holotype). No skulls of *Trogosus* other than those listed above are known at this time. Selected measurements of SDSNH 40819 and other specimens are shown in Table 1. Other comparative skull (Table S1), dental (Table S2), and cervical measurements (Table S3) are cited in Supplementary Data. In addition, the skulls of *Azygonyx ancylion* (UM 68511, holotype; see Gingerich and Gunnell, 1979), *Esthonyx acutidens* (USNM 18202, figured by Gazin, 1953), and *Tillodon fodiens* (YPM 11087, holotype), which preserve a number of diagnostic morphological features, were utilized in comparative discussions of trogosine taxonomy. Morphological characters used in the phylogenetic analysis and listed in Appendix S1 of Supplementary Data are designated as such in the text with numbers in brackets (e.g., character 1, state 1 is written as 1[1]).

Anatomical Terminology—Wherever possible, nondental cranial terminology employed in this paper follows Wible (2003, 2008, 2011). These papers provide excellent descriptions of extant mammalian crania and utilize terminology largely based on the English equivalents of terms found in reports of the International Anatomical Nomenclature Committee (1983) and the International Committee on Veterinary Gross Anatomical Nomenclature (2012). These works also review anatomical terminology found in various other sources, including Evans (1993). Dental terminology follows that of Bown and Kraus (1979) and Miyata (2007b). However, the usage of 'parastyle' for the anterolabial stylar cusp on upper molariform teeth is recommended instead of stylocone, to avoid confusion with dental terminology used in previous tillodont papers (see also Wang and Jin, 2004; Miyata, 2007b).

Anatomical Abbreviations for Cranium—**as**, alisphenoid; **asc**, alisphenoid canal; **ats**, auditory tube sulcus (= sulcus of eustachian tube); **bo**, basioccipital; **bs**, basisphenoid; **ch**, choanae; **cpf**, caudal palatine foramen; **cs**, condyloid sinus; **dcf**, dorsal condyloid foramen; **eam**, external acoustic meatus; **ecp**, ectopterygoid process; **egp**, entoglenoid process; **enp**, entopterygoid process; **eo**, exoccipital; **eoc**, exoccipital crest; **fm**, foramen magnum; **fo**, foramen ovale; **fr**, frontal; **gf**, glenoid fossa; **gsa**, groove for stapedial artery; **hf**, hypoglossal foramen; **inf**, incisive foramen; **iof**, infraorbital foramen; **jf**, jugular foramen; **ju**, jugal; **lac**, lacrimal; **lacf**, lacrimal foramen; **mapf**, major palatine foramen; **mp**, mastoid process of petrosal; **mpfr**, maxillary process of frontal; **mx**, maxilla; **mxf**, maxillary foramen; **na**, nasal; **nu**, nuchal crest; **oc**, occipital condyle; **ocmp**, occipitomastoid process (= **mp** + **pcp**); **on**, odontoid notch; **pa**, parietal; **pal**, palatine; **pcp**, paracondylar process of exoccipital; **pdp**, posterodorsal process of premaxilla; **pf**, piriform fenestra; **pgf**, postglenoid foramen; **pgp**, postglenoid process; **pmx**, premaxilla; **pns**, posterior nasal spine; **pop**, postorbital process of frontal; **ppp**, palatine process of premaxilla; **pps**, posterior palatine sulcus; **ppt**, postpalatine torus; **pr**, promontorium of petrosal; **pt**, pterygoid; **ptfo**, pterygoid fossa; **ptp**, posttympanic process of squamosal; **rt**, foramen for ramus temporalis; **sc**, sagittal crest; **smc**, suprameatal crest of squamosal; **smf**, stylomastoid foramen; **so**, supraoccipital; **socf**, supraoccipital foramina; **sof**, sphenorbital fissure; **spf**, sphenopalatine foramen; **sq**, squamosal; **th**, tympanohyal; **tl**, temporal line; **vcof**, ventral condyloid fossa; **zpmx**, zygomatic process of maxilla; **zpsq**, zygomatic process of squamosal.

GEOLOGICAL SETTING AND COMMENT ON THE DELMAR FORMATION *HYRACHYUS*

The specimens of *Trogosus* (SDSNH 40819) and *Hyrachyus* (SDSNH 55276) collected at the Swami's Point locality, San Diego County, California, U.S.A. (Fig. 1), were recovered from angular beach cobbles and small boulders of gray green, fine-grained sandstone found resting on the present beach. The clasts were likely derived from spoils generated by excavations for a concrete footing to support a new beach access stairway constructed in late 1990. The excavations were made directly into strata of the Delmar Formation, which forms the modern marine abrasion platform and adjacent sea cliff in this area. Apparently, the spoils were left on the beach and subsequently reworked by wave action, which broke down larger sandstone blocks into angular cobble-sized blocks and scattered them along the beach for several hundred meters south of the stairway. The fossil-bearing beach clasts were collected during several visits to the site in February 1991.

Although the Delmar Formation is well exposed in the sea cliffs in the vicinity of the Swami's Point locality, the stratigraphic position of the vertebrate fossil-producing horizon can only be approximated, because repeated searching for the source strata proved fruitless. Even so, based on the stratigraphic section exposed in the area, it is clear that the fossils were derived from the upper portion of the Delmar Formation, and from a

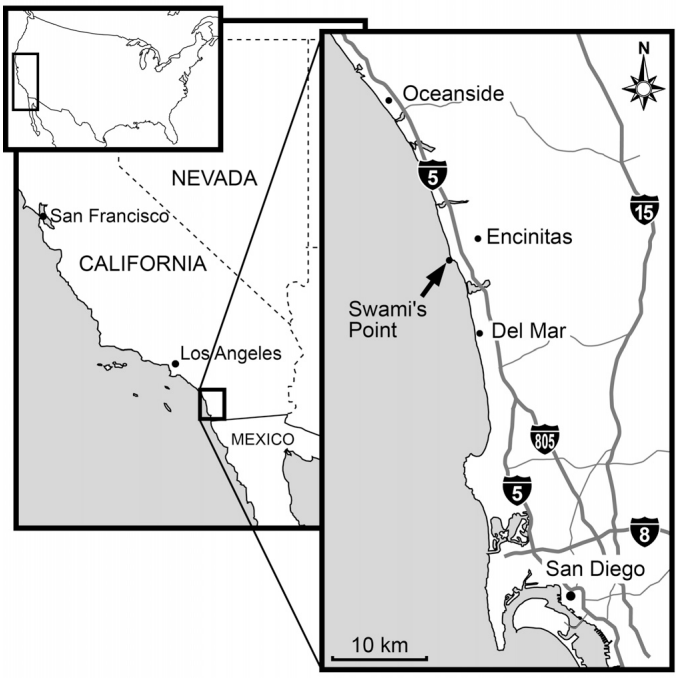

FIGURE 1. Map showing the location of Swami's Point (SDSNH loc. 3542), western San Diego County, California, U.S.A.

level less than 16 m below the gradational contact with the overlying Torrey Sandstone, which is exposed in the sea cliffs to the north of the stairway. Resistant shell beds dominated by disarticulated shells of the middle Eocene oyster, *Acutostrea idriaensis*, occur in this part of the Eocene section and are characteristic of the estuarine facies of the Delmar Formation (Moore, 1987; May and Warme, 1991; Warme, 1991).

The Swami's Point local fauna is most likely correlative with the Br2 biochron, upper Blacksforkian Subage, middle Bridgerian, as discussed by Robinson et al. (2004). A correlation web involving paleomagnetic (Flynn, 1986; Bottjer et al., 1991), superpositional (Walsh, 1996), and microfossil data (Bukry and Kennedy, 1969; May et al., 1991) suggests that the upper portion of the Delmar Formation was deposited near the early-middle Eocene (Ypresian-Lutetian) boundary. The open marine Ardath Shale, which unconformably overlies the Delmar Formation in the southern part of the Eocene San Diego embayment (Kennedy, 1975), has yielded nannofossils of the CP 12b subzone (Fig. 2; Bukry and Kennedy, 1969; May et al., 1991; Walsh, 1996). Magnetostratigraphic studies document a reversed polarity interval in the Delmar Formation and a normal polarity interval in the Ardath Shale and overlying Scripps Formation (Flynn, 1986; Bottjer et al., 1991). This magnetostratigraphic pattern has, in turn, been correlated with chrons C21r and C21n, respectively (Fig. 2; Robinson et al., 2004). At a minimum, the upper part of the Delmar Formation most likely falls within Chron C21r, which is currently correlated at ca. 48.57–47.35 Ma (Vandenberghe et al., 2012), latest early to earliest middle Eocene. Palynological data from Eocene formations in the San Diego area also suggest assignment of the Delmar Formation to the early middle Eocene (Frederiksen, 1991).

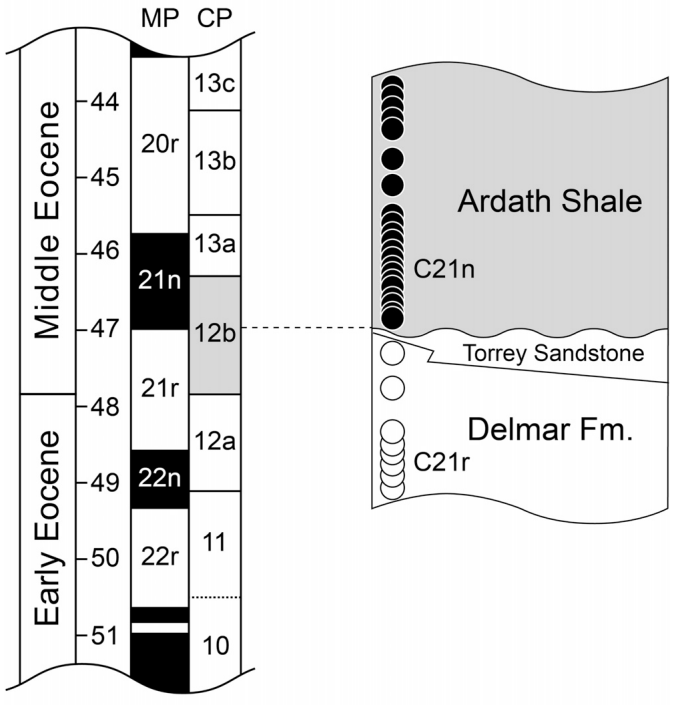

FIGURE 2. Correlation of the Delmar Formation with the standard global chronostratigraphic time scale (Vandenberghe et al., 2012), showing the interval of nannofossil subzone CP 12b and the magnetic polarities (MP) near the early-middle Eocene boundary. The magnetostratigraphic data and interpretation of the Ardath Shale and Delmar Formation are based on Bottjer et al. (1991).

Occurrence of *Hyrachyus modestus* (Leidy, 1870) in the Delmar Formation

Before turning to the description of the Delmar Formation *Trogosus*, it is worth commenting on the occurrence of *Hyrachyus* (*Hyrachyus* sp. in Walsh, 1996) in the Swami's Point local fauna and its biochronological implications. The specimen (SDSNH 55276) represents the posterior half of a well-mineralized skull preserving the region from the anterior rim of the orbits to the back of the occipital condyles (Fig. 3). Although the skull is slightly laterally deformed by compression, the basicranium is nearly complete. The left molars (M1–M3) provide a complete length of the molar series despite damage to the parastyles and paracones of M1–M2. The crown of the right M2 is also damaged, but the right M3 is complete. Each of the molars shows a bilophodont pattern with a protoloph and metaloph and a crest-like metacone. Labial and lingual cingula are lacking, except for a faint and discontinuous cingulum on the labial bases of the M1–M2 metacones. The M3 has a trapezoidal occlusal outline with short metaloph and postmetacrista. These molar features are consistent with those reported for species of *Hyrachyus* (e.g., Wood, 1934; Radinsky, 1966), supporting assignment of SDSNH 55276 to this genus. The M1 and M2 are relatively large (length × width in millimeters: M1, 19.2 × 20.9; M2, 20.4 × 21.6; M3, 17.5 × 20.7), with a combined anteroposterior length for the M1–M3 molar series of 56.8 mm. The latter measurement falls at the upper end of the diagnostic range (49–57 mm) of *Hyrachyus modestus* (Leidy, 1870) proposed by Wood (1934) and just outside the observed range (40–57 mm; mean = 49.29 ± 1.11, standard deviation = 5.43) of *H. modestus* reported by Radinsky (1967) for specimens from the lower Bridger Formation. Importantly, the M1–M3 length of SDSNH 55276 falls below the molar series lengths of specimens of the larger species, *H. eximius* Leidy (1871) (60–73 mm; mean = 64.35 ± 0.90, standard deviation = 3.71), as reported by Radinsky (1967). Thus, dental dimensions suggest assignment of SDSNH 55276 to a large individual of *H. modestus*.

Numerous specimens of *Hyrachyus* have been found in North America, but as noted by Schoch (1984) and Colbert and Schoch (1998), a thorough systematic revision of the genus is lacking. Wood (1934) proposed a classification for North American 'hyrachiids' that recognized four genera and 12 species. Since then, the only substantive study of this group has been that of Radinsky (1967), who revised its systematics to include only a single genus (*Hyrachyus*) with two North American species (*H. modestus* and *H. eximius*). Except for a discussion regarding the presence of a nasal rugosity, the species-level taxonomy proposed by Radinsky (1967) was based only on dental dimensions, which failed to support the qualitative morphological criteria (e.g., upper premolar cusp pattern) used by Wood (1934) (Schoch, 1984). More recently, Emry (1990) has supported the validity of *Hyrachyus affinis* (Marsh, 1871) as a smaller North American species than *H. modestus*. However, this recommendation still needs to be quantitatively tested. In conclusion, the Delmar Formation *Hyrachyus* is roughly intermediate between *H. modestus* and *H. eximius* in tooth dimensions, although closer to the former. At present, there is no justifiable reason for assigning it to a species other than *Hyrachyus modestus. Hyrachyus* has been reported from both the Bridgerian (*H. modestus*) and the Uintan (*H. eximius*) (Gunnell et al., 2009).

Hyrachyus modestus and species of *Trogosus* are known from Br1a–Br3 and from Br1a–Br2, respectively (Gunnell et al., 2009), although material of *Trogosus* is not abundant enough to use this taxon alone to recognize the Wasatchian-Bridgerian boundary in stratigraphic sections containing this taxon, in contrast to numerous occurrences of *Hyrachyus* (Smith and Holroyd, 2003). In summary, the co-occurrence of *Trogosus* and *Hyrachyus* strongly indicates a correlation of the Swami's Point

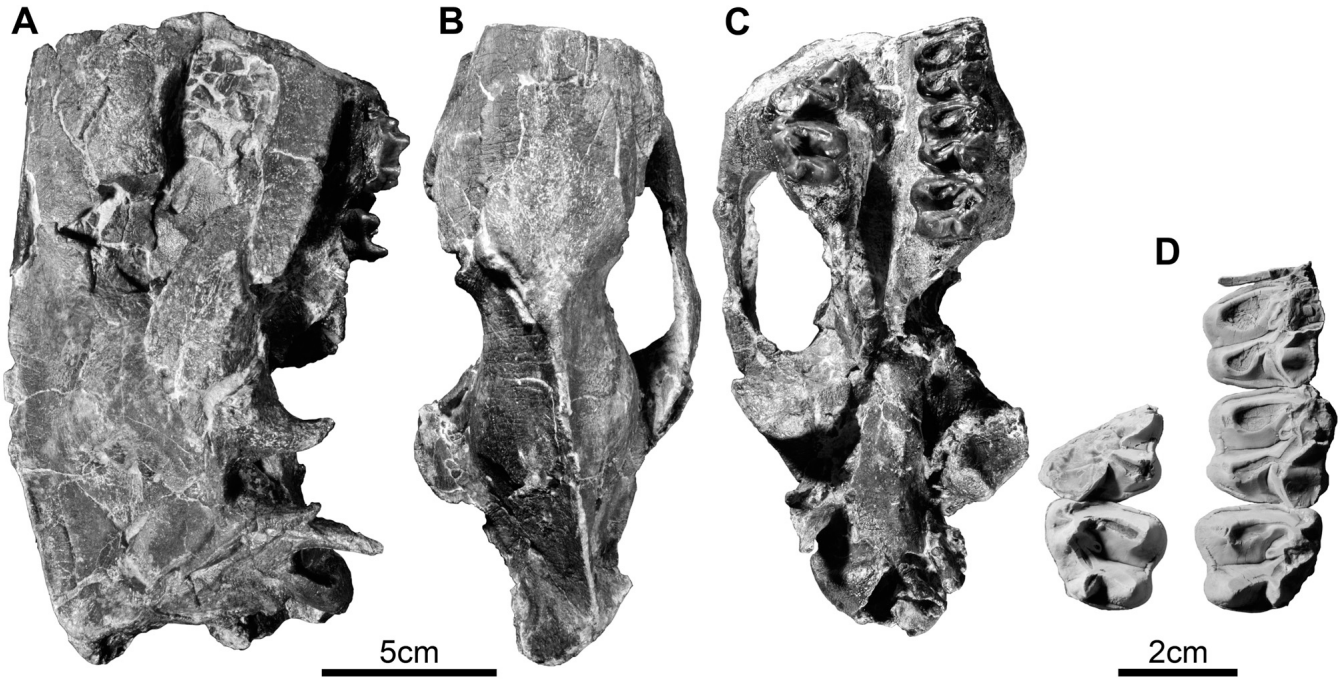

FIGURE 3. Partial referred skull of *Hyrachyus modestus* (SDSNH 55276) in right lateral (**A**), dorsal (**B**), and ventral (**C**) views. **D**, cheek teeth of SDSNH 55276, a fragment of left P4 and upper molars (partially damaged left M1–M3, right broken M2, and complete M3); coated with sublimated ammonium chloride, in occlusal view.

local fauna with the Bridgerian NALMA, most likely with Br2, considering that Br2 has been correlated with chrons C22n–C21r according to the most recent paleomagnetic calibrations of Tsukui and Clyde (2012).

SYSTEMATIC PALEONTOLOGY

Order TILLODONTIA Marsh, 1875
Family ESTHONYCHIDAE Cope, 1883
Subfamily TROGOSINAE Gazin, 1953
Genus *TROGOSUS* Leidy, 1871
TROGOSUS CASTORIDENS Leidy, 1871
(Figs. 4–6, 8, 9, 11–18)

Trogosus sp.: Walsh, 1996:77.

Type Material—ANSP 10337; incomplete and fused right and left dentaries with i2 and heavily worn m1–m2 and broken p4 and m3 (Gazin, 1953).

Type Locality and Horizon—Grizzly Buttes, southern Green River Basin (Bridger Basin), Uinta County, Wyoming; lower member of the Bridger Formation, Br2 (Gazin, 1976; Alexander and Burger, 2001; Gunnell et al., 2009).

Referred Material—SDSNH 40819; nearly complete skull with right and left I2s and P3–M3s, associated right I3 and left C1, proximal portions of right and left dentaries with m2–m3, incomplete stylohyoids, atlas, and three posterior cervical vertebrae.

Locality and Horizon—SDSNH locality 3542, about 200 m south of Swami's Point, Sea Cliff County Park, Encinitas, San Diego County, California (Fig. 1; 33°2′5″N, 117°17′32″W); upper part of the Delmar Formation. Locality 3542, which is placed within Chron 21r, seems to be almost coeval with, or slightly younger than the type specimen, because the Church Butte tuff interbedded in the Blacks Fork Member is dated as 49.05 ± 0.16 Ma ($^{40}Ar/^{39}Ar$ dating by Smith et al., 2008, 2010) and is placed within a normal interval calibrated to Chron C22n (Tsukui and Clyde, 2012).

Emended Differential Diagnosis—*Trogosus* species having a short and shallow rostrum (= short I2–P2 distance or i2–p3 distance), a vestigial (or possibly lost) i3, a short maxilla-nasal suture (point-like contact between nasal and maxilla), a narrow palatal flexion between the horizontal and perpendicular processes of palatine, a low sagittal crest, a narrow odontoid notch between occipital condyles, and a dorsoventrally shallow dentary. A lingual groove in the m3 talonid extending from between entoconid and hypoconulid also might be diagnostic of *T. castoridens*.

Distinguished otherwise from *Trogosus hyracoides* in having a smaller and lower P3 parastyle, an M3 smaller than M2, a more anteriorly extending palatine process of premaxilla, a facial process of lacrimal extending anterior to orbital rim, and a lacrimal foramen positioned on anterior orbital rim. Because the possibility exists that *T. hyracoides* and *T. castoridens* might represent sexually dimorphic members of a single species (see discussion below), the differences between these taxa may represent intraspecific variation.

Differs from *Trogosus grangeri* and *T. hillsii* in having a sigmoid premaxilla-maxilla suture, a narrow posterodorsal process of premaxilla, a slightly convergent anterior nasal process, a deep nasal intrusion into frontals, a 'V'-shaped frontonasal suture, a short nasal intrusion into maxilla-frontal suture, a posteriorly positioned anterior margin of choanae, no lacrimal tubercle above lacrimal foramen, a narrow jugal with an acute masseteric margin, a relatively longer dorsal portion of frontal, a long supraorbital rim, a posteriorly narrower dorsal portion of parietal forming lateral surface of braincase, a posterior opening of alisphenoid canal as large as the foramen ovale, a transversely wider postglenoid process of squamosal, a knob-shaped (bulbous) occipitomastoid process, and a quadrate ventral basioccipital with parasagittal edges extending from each occipital condyle.

In addition, further differences from *T. grangeri* include a weak margin of external nares, a less laterally expanded zygomatic arch, a posteriorly positioned zygion, a shallower pterygoid, and no midline crest (ventral keel) on basisphenoid.

Differs from *Trogosus latidens* and *T. gazini* in having a crest-like P3 parastyle and a less asymmetric pattern formed by lingual crests (less expanded postprotocrista) of P4. Further differences from *T. latidens* include its overall smaller size (see also Miyata, 2007a) and possession of a short diastema anterior to p3. Other differences from *T. gazini* include an M3 smaller than M2, a moderately larger m2 compared with m1, no basin structure between m2 hypo- and entoconids, and no distinct m3 posthypocristid (see also Miyata, 2007b).

DESCRIPTION AND COMPARISON

Skull

Overview—The skull of SDSNH 40819 is nearly complete, missing only the anterior extremities of the nasals, the anterodorsal parts of the premaxillae housing the I2s, the dorsolateral part of the right frontal, and portions of the right squamosal and jugal (Fig. 4). The dorsal margin of the sagittal crest is abraded, as is the dorsal margin of the lambdoidal crests. Diagenetic changes, primarily from dorsoventral compression (caused by stratigraphic load), have collapsed the orbital and temporal regions of the frontals, parietals, and squamosals against the underlying, ventral portions of these skull bones. This compression caused a longitudinal breakage of the temporal wall from the parietosquamosal suture to the lacrimal and thus conceals the temporal plate of frontal and parietal. The palate has also been slightly deformed by this dorsoventral compression, as reflected by a greater degree of dorsal arching and breakage and opening of the intermaxillary suture along the midline (Fig. 5). In spite of these condition issues, the skull is possibly the most complete trogosine skull known.

In general form, and in spite of the diagenetic distortion, the skull represents a rather slender species of *Trogosus* with a relatively shallow and short rostrum (i.e., short-faced) (Tables 1, S1). The rostrum (premaxilla + maxilla) is dorsoventrally shallow (character 33[0]); the depth of the rostrum is approximately 70% of that of *T. hyracoides* and *T. hillsii* and approximately 62% of that of *T. grangeri* (Table 1), and the premaxillary length is approximately 78% of that of *T. hyracoides* and *T. grangeri*. The anterior portion of the rostrum, between the labial sides of both I2s, is narrower than in *T. grangeri* (45.2 vs. 51.7 mm, approximately 14.4% wider) and similar to *T. hyracoides* (44.5 mm). However, the rostral width at the C1s (56.7 mm) does not distinctly differ from this dimension in other species of *Trogosus* (Table 1).

Narial Aperture and Premaxilla—The paired premaxillae of SDSNH 40819 are dorsoventrally shallow and form a relatively small external nasal aperture (external nares); the diameter of the external nares from the anterior extremity of the premaxilla to the anterior-most end of the premaxilla-nasal suture (as preserved) is shorter than that of *T. hyracoides* (29% longer) and *T. grangeri* (39% longer). The premaxillary margin of the external nasal aperture is damaged but seems to be gracile as in *T. hyracoides*, in contrast to the condition in *T. grangeri* where the premaxillary margin forms a stout, ridge-like rim (character 37). At the front of the palate, the anterior border of the paired premaxillae possesses a wedge-shaped, posteriorly directed, midline notch (= palatal notch of Gazin, 1953) between the I2s, as seen in other species of *Trogosus*.

The premaxilla of SDSNH 40819 extends posteriorly to the level of the posterior margin of P4, as seen in other species of *Trogosus*. The posterodorsal process of the premaxilla extends almost to the maxillary process of the frontal (Figs. 4, 6), but makes no direct contact with the frontal. Instead, a very short (left) to nonexistent (right, a point-like contact) maxilla-nasal suture intervenes between the premaxilla and frontal (character 42[2]; see also Maxilla section). As in *T. hyracoides*, the posterodorsal process of the premaxilla is transversely narrower than the condition in *T. grangeri* and *T. hillsii* (character 35[1]). Gazin (1953) noted that the premaxilla-maxilla suture in trogosine tillodonts extends obliquely across the rostrum from its posterior end to a midpoint between I3 and C1. However, as noted here, the suture condition varies among trogosine species (character 34). The premaxilla-maxilla suture in SDSNH 40819 has a sigmoid outline on the lateral side of the rostrum, marked by a distinct right-angled deflection positioned slightly above the level of the

TABLE 1. Selected measurements (in mm) of cranium and dentary of SDSNH 40819, *Trogosus castoridens*, and other species of *Trogosus* and *Tillodon*.

Dimension	*T. castoridens* SDSNH 40819	*T. hyracoides* USNM 17886	*T. grangeri* AMNH 17008	*T. hillsii* USNM 17157	*Tillodon fodiens* YPM 11087
Cranium					
Condylobasal length	258.4	—	280.7	—	342.1a
Palatal length	140.4	157.2	149.2	—	192.8
Distance between lacrimal foramen and postorbital process	37.6	46.2	30.2	27.7	22.8
Nasal length	99.1a	122.7	108.3a	—	140.0g
Width of rostrum at C1	56.7	57.6	61.8	57.5a at P2–P3	81.1
Width across postorbital processes	82.0a	77.5	102.2	79.8	135.2
Bizygomatic width (greatest skull width)	187.6a	176.0a	217.6	178.2a	210.3a
Biparietal width at squamosal contact (width of braincase)	39.5	38.4	58.6	46.4	74.2
Width of choanae	21.3	19.0	24.4	24.1	25.2
Width between occipital condyles	43.3	—	52.4	49.4	58.9
Depth of rostrum at P2–P3	37.7a	54.3	60.8	54.1	63.6
Height of occiput, above ventral margin of condyles	58.7*	—	97.8	68.4*	89.3
Depth of jugal anterior to zygomatic process of squamosal	13.7	22.6	19.0	18.2	19.2
Depth of zygomatic process of squamosal at glenoid fossa	21.8	29.8	34.6	—	29.5
Width × height of infraorbital foramen	5.6a in diameter	8.8 × 6.9	13.4 × 6.6	11.8 × 6.6	12.1 × 10.5
I2–P2 distance, ratio for P3–M3 length	40.7, 0.54	50.0g, 0.59	55.0g, 0.65	21.5 at I3–P2	61.0ag, 0.71
Dentary					
i2–p3 distance, ratio for p3–m3 length	(19.0ag, 0.22)	27.3g, 0.30	34.0g, 0.38	24.0ag, 0.27	38.0g, 0.41
Depth of dentary at m2–m3, internal	49.2 (46.0g)	55.0ag	58.0g	52.0g	66.0g (63.5g)
Thickness of dentary at m2	20.4 (21.5g)	23.5g	22.5g	23.0g	28.0g (24.5g)

*and 'a' indicate actual dimensions measured at broken portions and estimated dimensions, respectively. 'g' indicates the measurement from Gazin (1953). Average is cited here when the measurements on right and left sides are available. Measurements in parentheses of *T. castoridens* and *Tillodon fodiens* are based on ANSP 10337 (holotype) and USNM 18164 (paratype), respectively.

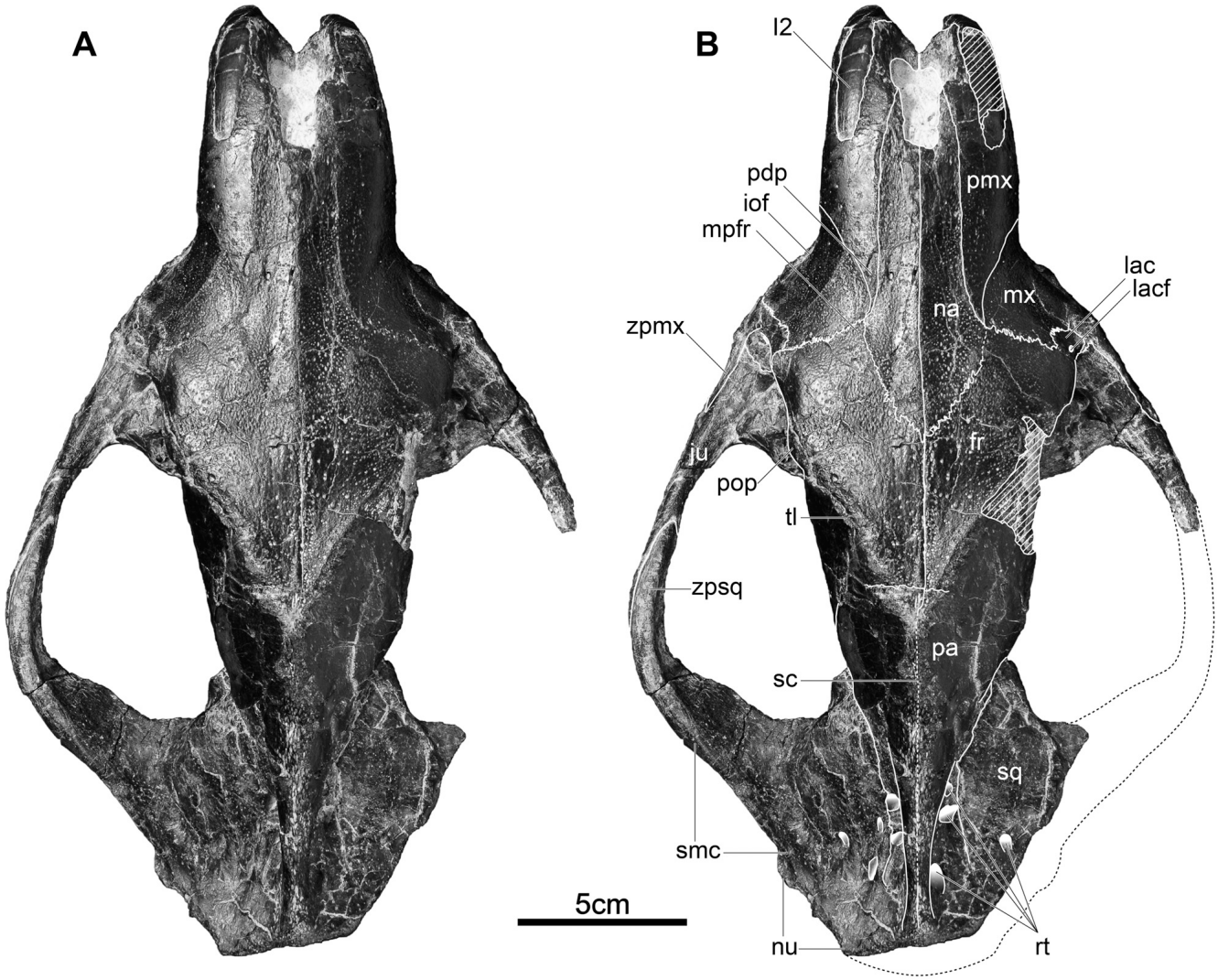

FIGURE 4. Referred skull of *Trogosus castoridens* (SDSNH 40819) in dorsal view. **A**, unlabeled; **B**, labeled with anatomical abbreviations used in text. White hatching indicates breakage.

infraorbital foramen (Fig. 6). In *Trogosus grangeri* and *T. hillsii*, the premaxilla-maxilla suture is nearly straight or only slightly deflected (Fig. 7B, D). In *Tillodon fodiens*, the premaxilla-maxilla suture has a conspicuous sigmoid-shaped outline with an intricate subvertical suture (Fig. 7H). The premaxilla-maxilla suture in SDSNH 40819 delimits the posterior margin of the I3 alveolus (Fig. 5) as in *T. grangeri* and *T. hillsii* (i.e., the maxilla forms the posterior border of the I3 alveolus), whereas this suture in *T. hyracoides* lies midway between the I3 and C1.

The ovoid incisive foramina in SDSNH 40819 are shorter than in *T. hyracoides* and narrower than in *T. grangeri* (Fig. 5). These size and shape differences of the foramina may be related to the shortness of the rostrum. The palatine process of the premaxilla forming the medial borders of the incisive foramina extends posteriorly to the level of the midpoint of I3 (Fig. 5), in contrast to the condition in *T. grangeri* and *T. hyracoides* where the process extends beyond the level of the posterior end of I3, as in *Tillodon fodiens* (character 36).

Nasal—Although the anterior margins of the nasals are damaged in SDSNH 40819, the anterolateral corners where the nasals contact the premaxillae are preserved. The nasal-premaxilla sutures are smooth, whereas the nasal-frontal sutures are finely serrated. The length of the paired nasals occupies approximately 38% of condylobasal skull length, and together the nasals deeply intrude posteriorly into the frontals (about 31% of the nasal length), as in *T. hyracoides* (Figs. 4, 7E; character 39[1]). The posterior border of the paired nasals has an intricate suture, forming a posteriorly directed and roughly 'V'-shaped wedge between the frontals (Fig. 4; character 40[0]). The nasals form a similar 'V'-shaped wedge between the frontals in *Tillodon fodiens* (Fig. 7G), although SDSNH 40819 has no lateral expansion of the nasals between the maxilla and frontal as in *T. hyracoides* (Figs. 4, 7E; character 41[0]). In contrast, the posterior margin of the paired nasals in *T. grangeri* and *T. hillsii* is bluntly rectangular (Fig. 7A, C; character 40[1]; Gazin, 1953). The posterior nasal intrusion in SDSNH 40819 extends to a level anterior to the postorbital process of the frontal as in *T. hillsii* (Figs. 4, 6, 7C), whereas the paired nasals of *T. hyracoides* extend posterior to the level of the postorbital process (Fig. 7E). The paired nasals have subparallel lateral margins in SDSNH 40819 and become slightly narrower anteriorly as in *T. hyracoides* (Figs. 4, 7E; character 38[1]). The paired nasals are widest at

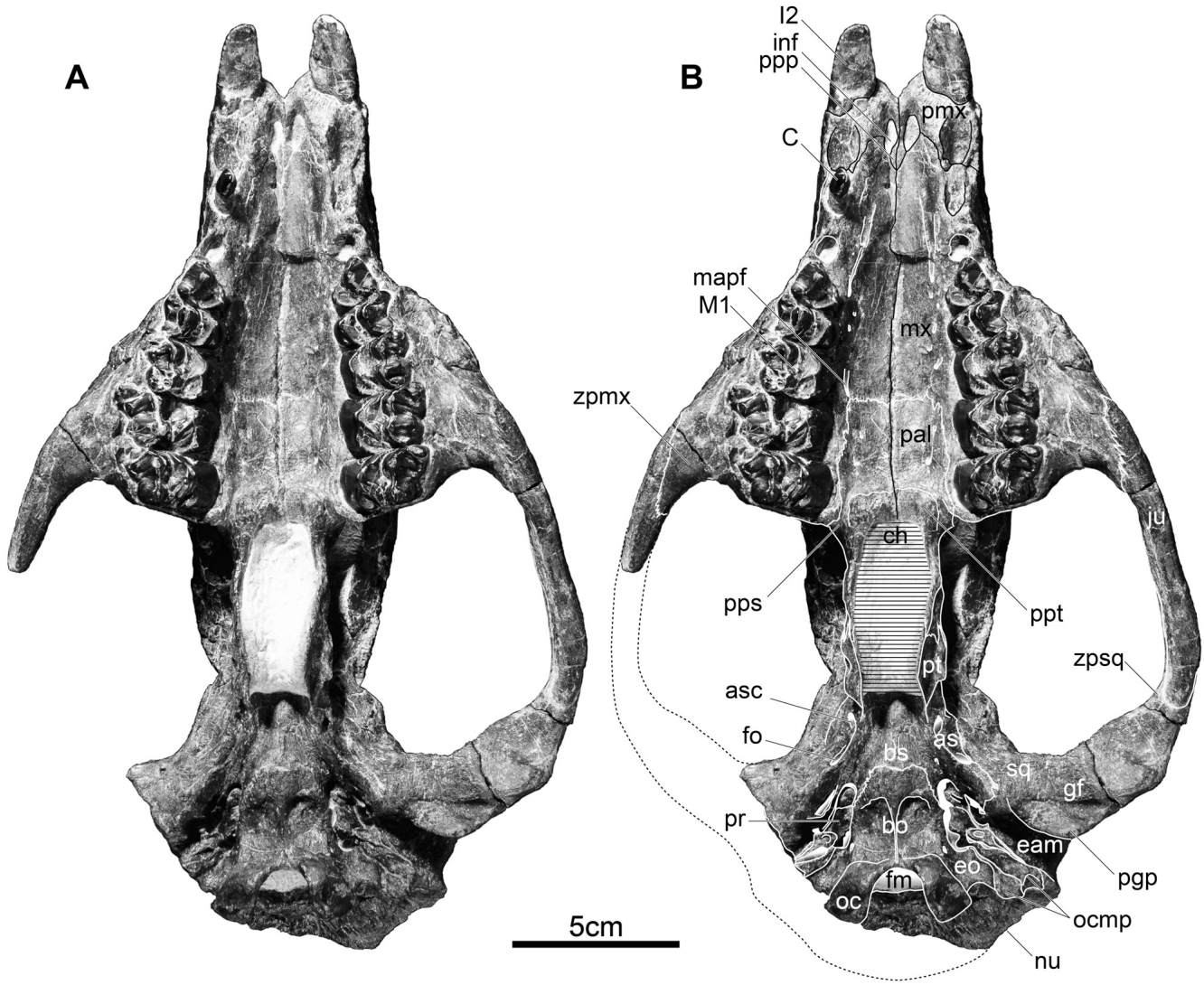

FIGURE 5. Referred skull of *Trogosus castoridens* (SDSNH 40819) in ventral view. **A**, unlabeled; **B**, labeled with anatomical abbreviations used in text. Black hatching indicates matrix in the choanae.

their contact with the maxillae (or between the maxilla-frontal sutures; Fig. 4). The paired nasals of *T. grangeri* (possibly also those of *T. hillsii*) do not anteriorly converge, but instead have parallel lateral margins (character 38[0]). A few tiny foramina asymmetrically arranged on either side of the midline are present on the nasals in SDSNH 40819 (also present in *T. grangeri*).

Maxilla—The maxilla of SDSNH 40819 is slender (width of rostrum and bizygomatic width in Table 1, palate width in Table S1). The infraorbital foramen is located dorsal to the posterolingual root of P3 as customarily positioned in other *Trogosus* skulls (Fig. 6D), and the openings of the infraorbital and maxillary foramina were dorsoventrally compressed during diagenesis. The infraorbital foramen, estimated to 5.6 mm in diameter, seems to be comparable to the nearly circular foramen of *T. hyracoides* and is smaller than the oval foramina of *T. grangeri* and *T. hillsii* (Table 1; character 43).

The maxilla of SDSNH 40819 has a very short (left) to almost nonexistent (right, point-like) contact with the nasal at its dorsalmost corner, whereas a longer and more distinct maxilla-nasal suture is present in other *Trogosus* skulls (Fig. 7; character 42). This feature may also be related to the shortness of the rostrum. The maxilla-premaxilla suture on the lateral side of the rostrum is smooth, whereas the maxilla-frontal and maxilla-lacrimal sutures are finely serrated. Each zygomatic process is smoothly continuous with the lacrimal in front of the lacrimal orbital rim through the serrated suture; therefore, the maxilla, as in *T. grangeri* and *T. hillsii*, does not contribute to the orbital rim. In *T. hyracoides*, owing to the presence of the concave lacrimal, the posterodorsal edge of the zygomatic process where it contacts the anterior margin of the lacrimal forms a part of the anterior orbital rim (Fig. 7F; character 49; see Lacrimal section) (Gazin, 1953).

The zygomatic process of the maxilla in SDSNH 40819 has a slightly wider facial surface compared with that in *T. grangeri* or *T. hillsii* (Figs. 6, 7). The posterior portion of the zygomatic process of the maxilla is developed as a thin sliver of bone that contacts the jugal to form a bifurcate, mortised suture. As in *T. hyracoides*, the zygomatic process of the maxilla in SDSNH 40819 has an acute masseteric margin (ventral ridge) that continues posteriorly onto the jugal. Furthermore, the maxilla of *T. hyracoides* has a wide facial surface above the upper cheek teeth, and a shallow depression

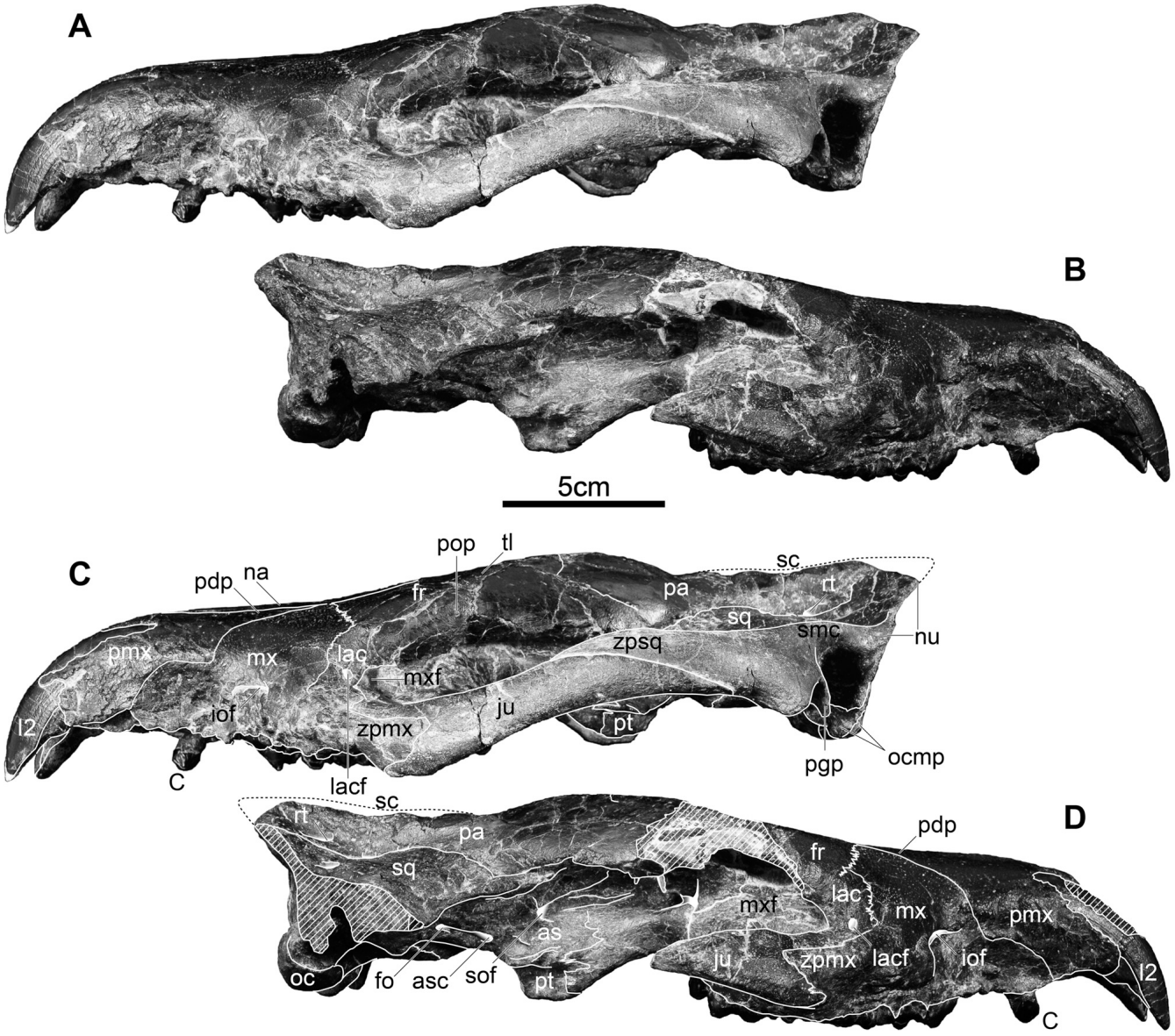

FIGURE 6. Referred skull of *Trogosus castoridens* (SDSNH 40819) in left (**A, C**) and right (**B, D**) lateral views. **A, B**, unlabeled; **C, D**, labeled with anatomical abbreviations used in text. White hatching indicates breakage.

between the zygomatic and alveolar processes above M2–M3. The maxilla of SDSNH 40819 also has a wide facial extent with a similar depression above M2–M3, although it is dorsoventrally deformed. These conditions of the zygomatic process and facial surface of maxilla suggest possible differences in development of the masseter muscles among the *Trogosus* species (Figs. 5–7; character 52; see Jugal section). In dorsal view, the paired maxillae of SDSNH 40819 are gently constricted transversely anteroventral to the infraorbital foramen. However, unlike the condition in *T. grangeri*, no distinct lateral concavity is present on the facial surface near the ventral border between C1 and P2 (character 45[0]).

In ventral view, the anteromedial border of the palatine process of the maxilla contacts the palatine process of the premaxilla and forms part of the posteromedial margin of the incisive foramen (Fig. 5). The paired palatine processes between the tooth rows gradually widen posteriorly, and except for the anterior narrowness of the processes, this feature does not differ from that of other species of *Trogosus*. The paired palatine processes preserve some accessory foramina, which are asymmetrically arranged on either side of the midline medial to P3 and P4. The distinct palatine foramen positioned anteromedial to P3 opens anteriorly into a shallow but distinct sulcus that extends forward to the level of C1 (Fig. 5). The palatine foramen with sulcus is customarily present medial to P3 in *T. hyracoides* and *T. grangeri*, whereas in *Tillodon fodiens* the palatine foramen lies medial to P2 (character 44; Gazin, 1953). Each posterior-most palatine foramen (= posterior palatine foramen of Gazin, 1953) is small and situated close to the transverse palatomaxillary suture on the right side and medial to the M1 protocone on the left side. Similar palatine foramina are asymmetrically positioned near or in the transverse palatomaxillary suture in *T. hyracoides* (the left one in the palatomaxillary suture) and *T. grangeri* (the right one just anterior to the suture). In SDSNH 40819, the palatomaxillary suture is somewhat irregular and positioned at the level between the M1 and M2. Posteriorly, the

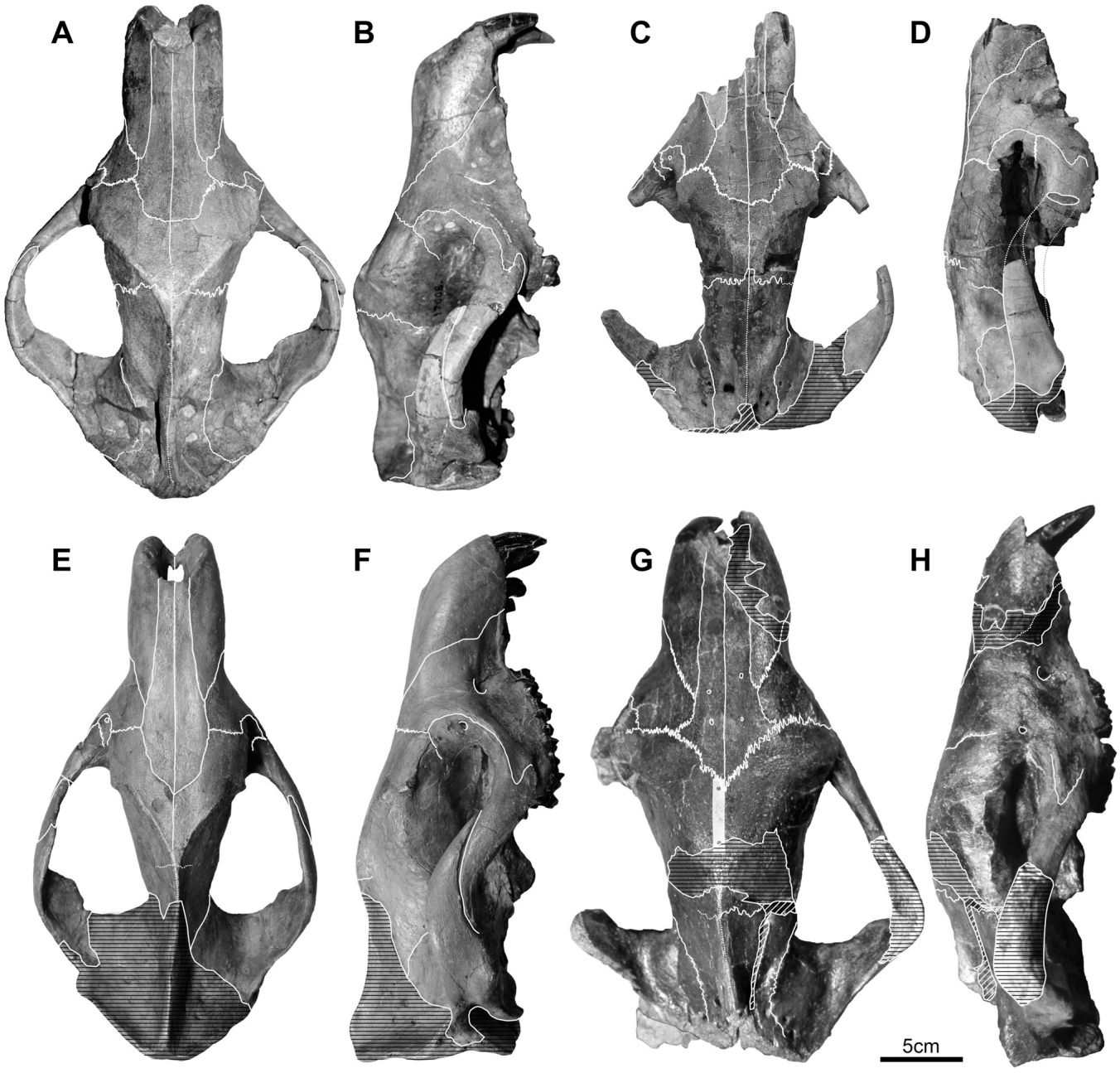

FIGURE 7. Skulls of trogosine tillodonts in dorsal (**A, C, E, G**) and right lateral (**B, D, F, H**) views. White and black hatching indicate breakage and reconstruction, respectively. **A, B**, *Trogosus grangeri* (AMNH 17008, holotype); **C, D**, *Trogosus hillsii* (USNM 17157, holotype); **E, F**, *Trogosus hyracoides* (FPDM-V 7824, cast of USNM 17886); **G, H**, *Tillodon fodiens* (YPM 11087, holotype).

suture becomes more parasagittally oriented in its extension towards the orbitotemporal fossa.

Palatine—The palatal surface (horizontal process) of the palatine occupies about 30% of the midline palatal length in SDSNH 40819 (Fig. 5). The extent of the horizontal process is relatively greater than that in *T. grangeri* and *T. hillsii*. In the latter two species, the anterior margin of the choanae (back edge of the horizontal process) extends more anteriorly, reaching the level of the M3 paracone (character 46[1]). As in *T. hyracoides*, the choanae of SDSNH 40819 are relatively narrower transversely (Table 1), with its anterior margin positioned at the level of the posterior wall of M3.

Five visible palatine foramina are present on the horizontal process, four of which are symmetrically arranged on either side of the midline: one pair of foramina positioned medial to the M2 and the second pair positioned at the level of the contact between M2 and M3. This arrangement is almost the same as in *T. hyracoides*. In *T. grangeri*, the posterior pair of foramina is positioned more medially.

The posterior border of the horizontal process has a postpalatine torus that becomes weaker medially (Fig. 5). Just lateral to the postpalatine torus, there is a narrow sulcus (= posterior palatine sulcus; Fig. 5), which continues to a saddle-shaped flexion between the horizontal and perpendicular processes. The

posterior palatine sulcus, possibly associated with the minor palatine nerve, is much broader in *T. hyracoides* and *T. grangeri* than in SDSNH 40819 (character 47[0]). *Trogosus grangeri* bears a small foramen in this sulcus. The posterior nasal spine of the choanae is weak in SDSNH 40819 (Fig. 8), as in *T. hillsii*, and is more clearly recognizable in the matrix filling the choanae based on computed tomography (CT) data. The posterior nasal spine is relatively stouter in *T. hyracoides* and *T. grangeri* (Gazin, 1953).

Although partially concealed due to post-depositional deformation, the perpendicular process of the palatine is a long and plate-like structure forming a complex suture with the alisphenoid and pterygoid (Figs. 6, 8). The ventral margin of the perpendicular process gradually descends posteriorly in SDSNH

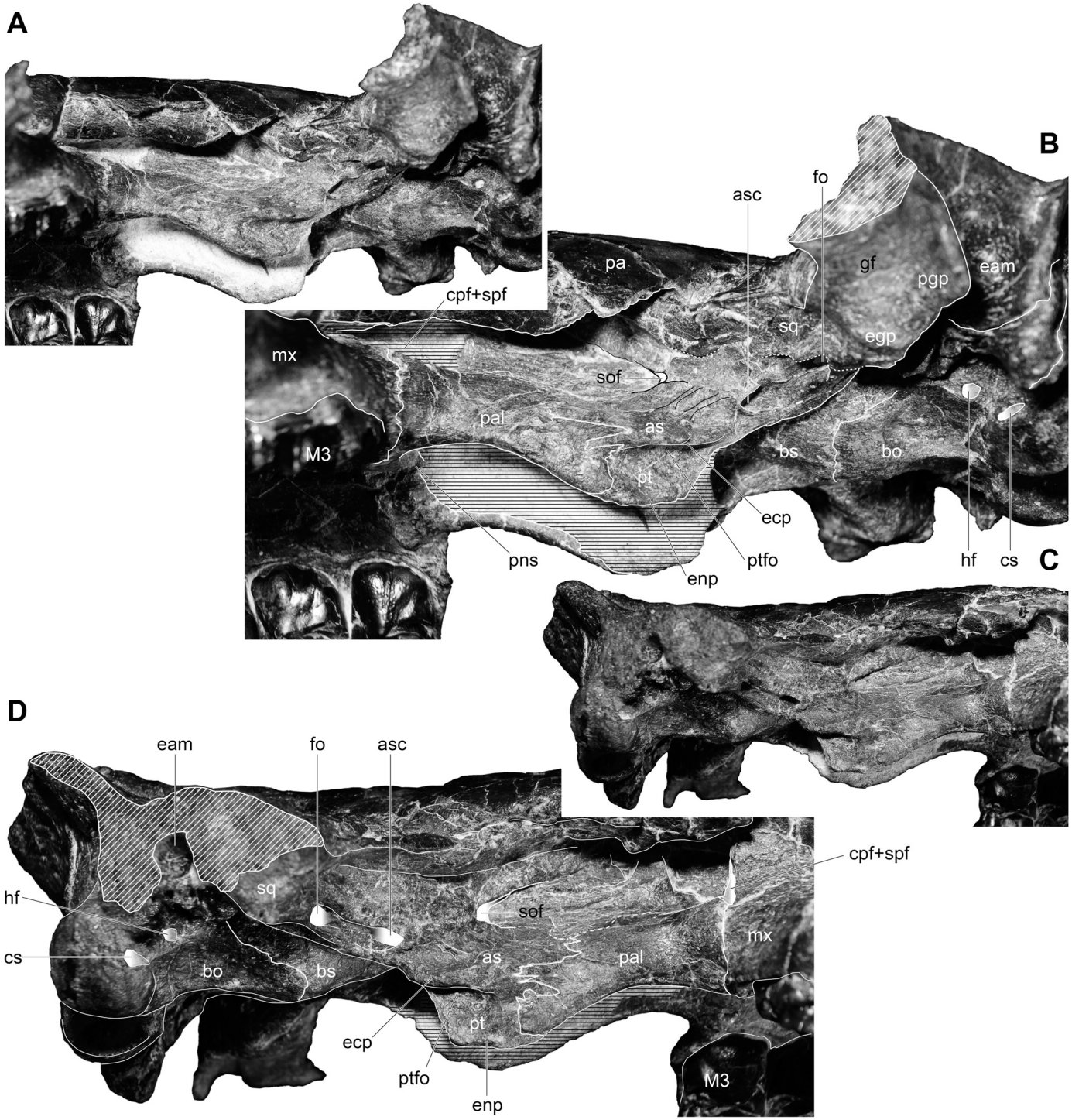

FIGURE 8. Basicranium of referred skull of *Trogosus castoridens* (SDSNH 40819) in oblique left lateral (**A, B**) and oblique right lateral (**C, D**) views (zygomae removed). **A, C**, unlabeled; **B, D**, labeled anatomical abbreviations used in text. Not to scale. White and black hatching indicate breakage and matrix, respectively.

40819, unlike the condition in *T. grangeri* where the perpendicular process forms a convex ventral outline with the deeper pterygoid in lateral view (Figs. 6, 7B, 8; character 62). The palatomaxillary suture in SDSNH 40819 extends parasagittally from behind the M3 into the orbital fossa (Fig. 8B). The sutures between the perpendicular process and the adjacent lacrimal, frontal, and orbitosphenoid are poorly defined. However, the pterygoid-alisphenoid suture is clearly represented by a squamous suture (Fig. 8). Each perpendicular process of SDSNH 40819 shows a large recess (foramen) near the palatomaxillary suture above the saddle-shaped flexion of the posterior palatine sulcus. This recess appears to contain the caudal palatine and sphenopalatine foramina (Fig. 8), as suggested by Gazin (1953). The recess in other species of *Trogosus* opens almost at the same position within the perpendicular process. Gazin (1953) noted that the sphenopalatine foramen in *T. hyracoides* is separated by a septum within the recess.

Lacrimal—The right lacrimal of SDSNH 40819 is better preserved and includes a narrow facial process anterior to the orbital rim (Figs. 4, 6). The anterior suture with the maxilla is well defined, but the sutures with other adjacent elements are unclear. The lacrimal foramen is positioned within the facial process, almost on the orbital rim, as also seen in *T. grangeri* and *T. hillsii*. However, the foramen is smaller in SDSNH 40819 and directed more medially (Fig. 6). The facial process in SDSNH 40819 is narrow and differs from that in *T. hyracoides*, in which the lacrimal is laterally concave with its anterior border with the maxillary zygomatic process forming a part of the anterior-most orbital rim (characters 49[1], 50[2]). The lacrimal tubercle (lachrymal process of Gazin, 1953) is absent in SDSNH 40819 and *T. hyracoides*, differing from the condition in *T. grangeri* (prominent tubercle) and *T. hillsii* (faint tubercle) (character 51). The poorly preserved left lacrimal of SDSNH 40819 shows a small bony protuberance at the contact with the maxilla-frontal suture, which is likely a result of post-depositional deformation.

Jugal—The jugal portion of the zygomatic arch is relatively straight and slender in SDSNH 40819 (Table 1, depth of jugal), and less laterally expanded than in the more curved and stouter zygomatic arch of *T. grangeri* (Figs. 4, 7; character 53). The anterior portion of the jugal where it contacts the maxilla has an acute masseteric margin (ventral ridge) in SDSNH 40819, in contrast to the more rounded ventral margin found in *T. grangeri* and *T. hillsii*. The condition in the latter taxa may reflect differences in the relative development of the anterior lateral masseter (character 52; see also Maxilla section). The zygion, the most lateral portion of the zygomatic arch, is located approximately in the posterior third of the arch, which is on the posterior end of the jugal (character 54[1]). As a consequence, the orbitotemporal fossa as defined by the zygomatic arch is roughly oval, as also seen in *T. hillsii* and *T. hyracoides*, whereas the condition in *T. grangeri* consists of a more circular orbitotemporal fossa, a result of the more anteriorly positioned zygion (Fig. 7).

The anterior portion of the jugal of SDSNH 40819 exhibits a bifurcate, mortised suture with the maxilla as seen in other species of *Trogosus*. Posteriorly, the jugal tapers in height, rather than in width, and gently curves dorsally to contact the squamosal (Fig. 6). The contact with the squamosal becomes slightly broadened at its midpoint. In *T. grangeri* and *T. hyracoides*, the jugal forms a greater angle (ca. 50°) with the occlusal plane, posteriorly tapers in both height and width from the contact with the maxilla, and has a more dorsally curved posterior extremity (Fig. 7).

Frontal—In dorsal view, the paired frontals and the posterior portions of the nasals occupy the broad interorbital region of the skull. The anterior half of the frontal forms the supraorbital rim, extending from the contact with the lacrimal to the blunt postorbital process (Fig. 4). The posterior half of the frontal bears a weak temporal line (temporal crest) extending posteromedially from the postorbital process (Fig. 4). The temporal lines on both sides posteriorly converge to form a 'V'-shaped rim and continue posteriorly to merge with the sagittal crest at a point beyond the sinuous coronal suture (i.e., frontoparietal suture), which is barely visible in the vicinity of the sagittal crest. Unfortunately, post-depositional deformation of SDSNH 40819 has damaged the orbital and temporal portions of the lateral plates of both frontals, making comparisons with the frontals of other species difficult.

Trogosus grangeri and *T. hyracoides* possess distinct supraorbital rims with prominent postorbital processes. In contrast, the postorbital processes are blunt and weakly developed in SDSNH 40819 and *T. hillsii* (character 57). The frontal and the supraorbital rim are shorter dorsally in *T. grangeri* and *T. hillsii* compared with the condition in *T. hyracoides* and SDSNH 40819 (characters 55, 56). In *Tillodon fodiens*, the supraorbital rim is short, the postorbital process is weakly developed, and the anterior terminus of the indistinct temporal line is positioned near the anterior orbital rim (Fig. 7G).

Gazin (1953) considered the position of the coronal suture on the cranial vertex to be a characteristic feature in trogosine skulls and noted that, except in *T. grangeri*, the suture is located posterior to the anterior terminus of the sagittal crest (i.e., the posterior confluence of the temporal lines). In SDSNH 40819 the coronal suture is positioned anterior to the confluence of the temporal lines, as in *T. grangeri*. We suggest that the position of the coronal suture relative to the confluence of the temporal lines may be an ontogenetic feature, with an anterior position associated with juvenile individuals and a posterior position associated with more mature animals.

Parietal—Unfortunately, post-depositional deformation has distorted the shape of the braincase, especially the configuration of the parietals on the lateral wall of the braincase. The dorsal and posterior portions of the sagittal crest and the nuchal crest are also partially damaged.

In dorsal view, the paired parietals become narrow posteriorly and are transversely constricted at the anteroposterior midpoint of contact with the squamosal (Fig. 4). The sutures with the squamosal and supraoccipital around the nuchal crest are obliterated. However, if the sutural morphology observed in other species of *Trogosus* (*T. grangeri* and *T. hillsii*) is applicable, the parietals of SDSNH 40819 seem to become wider posteriorly from their most constricted part and to contribute (along with the supraoccipital) to the medial half of the nuchal crest. The nuchal crest of SDSNH 40819 is well developed as seen in other *Trogosus*, but is more convergent posteriorly with the squamosals than in *T. grangeri* and *T. hillsii* (Figs. 5, 7).

The paired parietals are similar to those in *T. hyracoides* in being distinctly narrow posteriorly and not produced as a bulge of the dorsolateral wall of the braincase (Table 1; character 59 [1]). As also seen in *T. hyracoides*, the parietals are constricted transversely at the midpoint of the contact with the squamosal (character 60[0]); *Tillodon fodiens* also shows a similar parietal morphology. In contrast, as noted by Gazin (1953), the parietals in both *T. grangeri* and *T. hillsii* bulge dorsolaterally, with a low, but prominent swelling that extends anteroventrolaterally in front of the parietosquamosal suture. This dorsolateral bulging of the parietals is probably a result of the expanded cerebral hemispheres.

The sagittal crest of SDSNH 40819 is moderate in length, composing about one-third the length of the midline of the skull, as in other species of *Trogosus*. The sagittal crest is considerably lower compared with the crests of *T. grangeri* and *T. hyracoides*, and this feature more closely resembles the condition in *T. hillsii* (character 61[1]). In addition, the sagittal crest in SDSNH 40819 is dorsally faintly concave in lateral profile (Fig. 6).

Several large vascular foramina, positionally related to rami temporalis, are present posteriorly on the parietals (three in the

left and two in the right) between the base of the sagittal crest and the squamosal (Fig. 4). The posterior foramen on each parietal is posterodorsally opened and bears a short sulcus. The vascular foramina on the parietals are larger and more distinct in *T. grangeri* and *T. hillsii* (Fig. 7). Several lesser foramina are within the adjacent squamosals (at least three in the left and one in the right). The suture between the right and left parietals is indiscernible in SDSNH 40819, and there is no evidence of an interparietal. The presence of an interparietal has not been confirmed in previous studies of *Trogosus* skulls (Gazin, 1953). The posterior suture with the occipital is also indistinguishable, owing mainly to sutural fusion. However, the holotype skull of *T. grangeri* preserves a faint suture between the parietal and occipital on each nuchal crest (Fig. 7; Gazin, 1953).

Sphenoid Complex and Pterygoid—Little is known of these elements aside from a few comments in Gazin (1953) in which he suggested that the sphenoid and pterygoids were not fully differentiated in the available trogosine skulls. According to Gazin (1953), in both *T. grangeri* and *T. hillsii*, the skull appears to have neither a foramen rotundum nor an optic foramen externally. Instead, Gazin (1953) suggested that the large sphenorbital fissure (= sphenoidal fissure) contained both the foramen rotundum and optic foramen, at least externally. In SDSNH 40819, a large sphenorbital fissure (Fig. 8) is located on either side of the most constricted cranial part above the ectopterygoid process of the alisphenoid (Fig. 8). This specimen also appears not to have any external aperture that can be unequivocally recognized as the foramen rotundum, optic foramen, or anterior opening of alisphenoid canal. In addition, the orbitosphenoid in SDSNH 40819, which cannot be clearly differentiated from adjacent temporal bones, probably extends anterior to the sphenorbital fissure like in many eutherian mammals (Novacek, 1986, 1993).

Gazin (1953) tentatively identified an ethmoidal foramen in *T. grangeri*, based on a feature located at the frontal-orbitosphenoid suture above the recess on the perpendicular process of the palatine (posterior palatine foramen in Gazin, 1953 = caudal palatine and sphenopalatine foramina in Fig. 8; see also Palatine section). Close examination SDSNH 40819 failed to reveal an ethmoidal foramen, but this may be due to poor preservation.

The alisphenoid is clearly discernible in SDSNH 40819 and forms a relatively large portion of the lateral surface of the braincase and the lateral wall of the nasopharyngeal meatus with the perpendicular process of palatine (Fig. 8). Although the exact location of the suture is ambiguous, the alisphenoid is anteriorly delimited from the palatine by a faint suture that is preserved around the anterior base of the ectopterygoid process (Fig 8; see also Palatine section). The suture with the pterygoid is fused on either side. The ectopterygoid process projects posterolaterally and is separated from the entopterygoid process of the pterygoid by a narrow pterygoid fossa (Fig. 8), as is also the condition in *T. grangeri* and *T. hyracoides*. In SDSNH 40819, weak single and double ridges project posterodorsally above the ectopterygoid process on the left and right sides, respectively (Fig. 8). No visible suture is present between the alisphenoid and squamosal on the right side. However, a crack positionally representing this suture can be traced on the left side (Fig. 8B, 9). Posterolaterally, this suture extends from the lateral side of the foramen ovale, through the medial corner of the glenoid process, and then presumably into the external acoustic meatus. A similar position of this suture is preserved on the *T. grangeri* holotype skull.

The posterior opening of the alisphenoid canal is located posterodorsal to the ectopterygoid process (Figs. 8, 9). This opening is larger in diameter and more separated from the foramen ovale than in *T. grangeri* (Figs. 9, 10; character 63[1]), rather than being similar in size as seen in *T. hyracoides*. Unlike in *T. grangeri*, SDSNH 40819 has a distinct channel between the alisphenoid canal and the foramen ovale, whereas a more distinct and longer depression is present in *Tillodon fodiens* (Figs. 9, 10; Gazin, 1953). The foramen ovale in SDSNH 40819 is positioned intermediate between the posterior extremity of the ectopterygoid process and the posteromedial corner of the glenoid fossa, as in *T. grangeri*, and unlike the condition in *T. hyracoides* where the foramen is closer to the glenoid fossa.

The entopterygoid process of the pterygoid in SDSNH 40819 is shallower than in *T. grangeri* and gradually faces posteromedially, with a gently curved posteroventral margin (pterygoid hamulus). Posteromedial to the channel between the alisphenoid canal and foramen ovale, the pterygoid continues to a low crest on the tympanic process of the alisphenoid, which forms the anteromedial border of the auditory tube sulcus (Fig. 9). This crest is posterolaterally continuous with the sharp, medial ridge of the slit-like postglenoid foramen (Figs. 9, 11; see also Squamosal section), although the tympanic process of the alisphenoid is merged with the basisphenoid on either side with no clear sutural delimitation.

The vomer, presphenoid, and medial surface of the pterygoid are not exposed in SDSNH 40819 because the interior of the nasopharyngeal meatus is filled with sedimentary matrix (Fig. 5). The basisphenoid widens posteriorly in ventral view, and the configuration of the contact between the alisphenoid and adjacent bones is almost unknown aside from a faint posterior suture with the basioccipital. The ventral surface of the basisphenoid is weakly bulging, with a subtle eminence on the midline (Fig. 9). Unlike the condition in *T. grangeri*, however, no midline crest (keel) is present on the ventral surface of the basisphenoid between the pterygoids (Figs. 9, 10; character 64[0]). Although the lateral margin of the alisphenoid is not clearly defined, the tympanic wing of the basisphenoid likely forms the bulk of the auditory tube sulcus. A tiny vascular foramen is present at the auditory tube sulcus, just medial to the foramen ovale (arrows in Figs. 9, 11). This foramen is slightly larger in *Tillodon fodiens*, but is indiscernible in *T. grangeri*.

Squamosal—The left squamosal in SDSNH 40819 is complete, whereas on the right side the zygomatic process and the dorsolateral margin forming the lateral nuchal crest are missing. The paired squamosals contribute to formation of the posterior walls of the braincase and lateral portions of the basicranium. As mentioned before, vascular foramina (three left and one right) are located within the left and right dorsal portions of the squamosals near the parietosquamosal suture. The dorsal, temporal portion of the squamosal shows a concave, triangular bony shelf that is posterolaterally bounded by the suprameatal crest of the zygomatic process (Fig. 4; character 65[1]) and contacts the parietal medially. Unlike in *T. grangeri* and *T. hillsii*, the squamosals exhibit a posteriorly narrowing and transversely short dorsal outline of the basicranium (Figs. 4, 7).

The lateral portion of the nuchal crest is entirely formed by the squamosal, as shown by the position of the near vertical squamosal-occipital suture on the occiput (see also Occipital section). The nuchal crest of the squamosal extends ventrolaterally past the junction with the suprameatal crest of the squamosal and then continues to the postympanic process, which forms the posterior wall of the external acoustic meatus (Figs. 6C, 9). As thus configured, the squamosal contributes to the bulk of the external acoustic meatus. As seen in *Tillodon fodiens*, the infundibulum of the meatus in SDSNH 40819 widens distally and becomes narrower proximally, unlike in *T. grangeri* (see Auditory Region section).

The zygomatic process of the squamosal in SDSNH 40819, especially above the glenoid fossa, is dorsoventrally shallower than in *T. grangeri* and *T. hyracoides* (Table 1, depth of the zygomatic process). The anterior extremity of the process reaches nearly to the level of the postorbital process of the frontal. The zygomatic process of the squamosal attenuates anteriorly where it forms an extensive overlapping suture with the posteriorly tapering zygomatic process of the jugal.

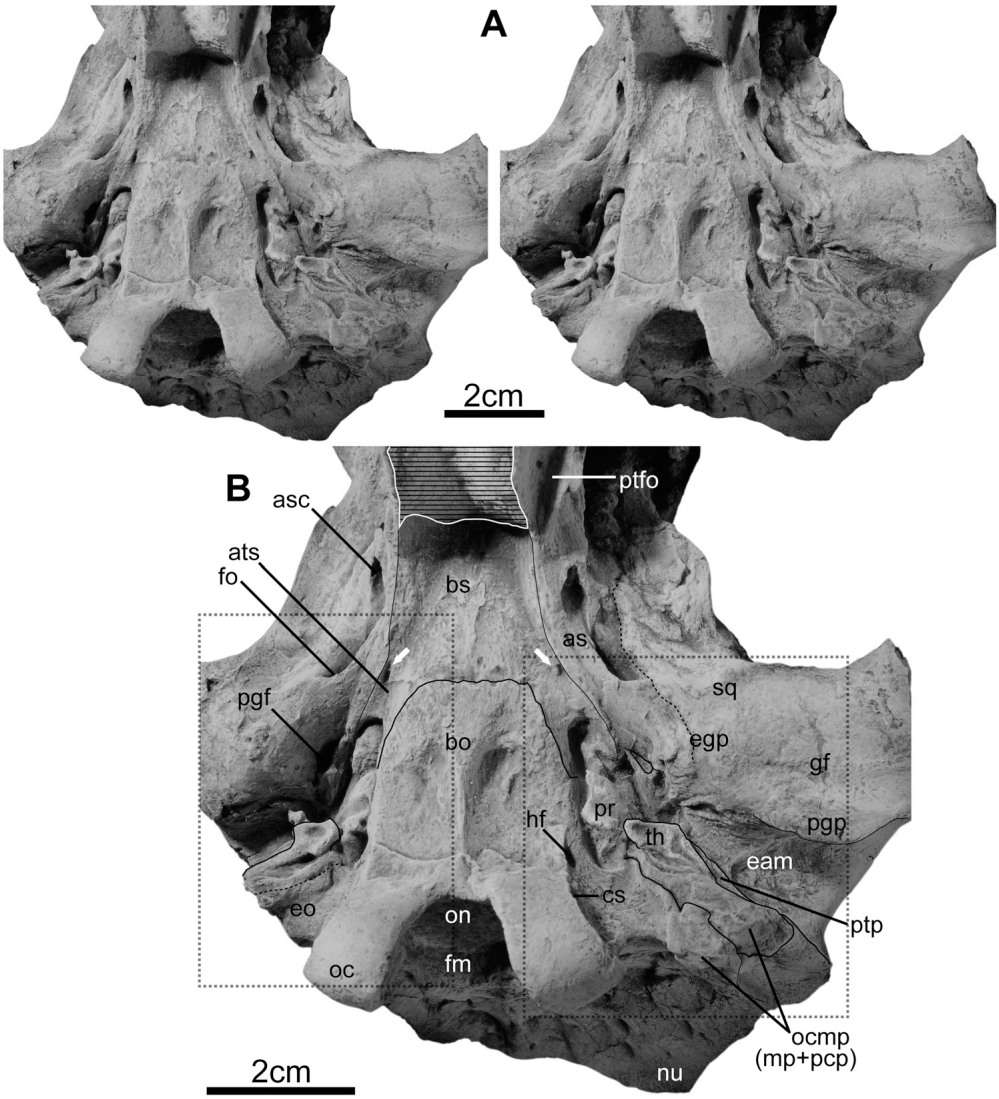

FIGURE 9. Basicranium of referred skull of *Trogosus castoridens* (SDSNH 40819), coated with ammonium chloride sublimate in ventral view. **A**, stereograph; **B**, labeled photograph with anatomical abbreviations used in text. Black hatching indicates matrix in the choanae. White arrows indicate foramina on the auditory tube sulci. Dotted lines indicate areas magnified in Figure 11.

Compared with other trogosine tillodonts, the lateral profile of the squamosal-jugal portion of the zygomatic arch in SDSNHM 40819 is relatively straight rather than dorsally arched (Figs. 6, 7).

In ventral view, the glenoid fossa of SDSNH 40819 is a roughly oblong articular surface with an almost planar medial half and becomes slightly wider laterally (Fig. 5). In *T. grangeri* and *T. hyracoides*, the glenoid fossa becomes slightly broader medially and is more concave. The long axis of the glenoid fossa in SDSNH 40819 is directed anterolaterally at about 65° from the midline of the skull. The medial corner of the glenoid fossa is marked by a low, pyramidal entoglenoid process (Figs. 8, 9). On the medial wall of the entoglenoid process, anterolateral to the promontorium of the petrosal, is a slit-like (transversely compressed) foramen set in a posterodorsally placed recess. This foramen is positionally assignable to the postglenoid foramen (Figs. 9, 11) and is most likely within the tympanic process of the alisphenoid near the assumed level of the alisphenoid-squamosal suture. A postglenoid foramen located in almost the same position occurs in *Trogosus grangeri, T. hillsii*, and *Tillodon fodiens*. However, in these taxa, the foramen is larger and more circular (Fig. 10). In *T. grangeri* and *T. hillsii*, a shallow vertical sulcus entering the postglenoid foramen is present on the medial wall of the entoglenoid process.

Another distinctive feature of the glenoid region in SDSNH 40819 is the transversely wide postglenoid process (Figs. 5, 9), which is an anteroposteriorly compressed, roughly triangular (in posterior view) ridge with a lateral extension rimming the majority of the posterior margin of the glenoid fossa (character 66[1]). A similar construction of the postglenoid process occurs on the left squamosal of *T. hyracoides*, although the right one is damaged. The postglenoid process of SDSNH 40819 is transversely wider than in *T. grangeri* and *T. hillsii* (Fig. 10) and possesses a shallow, transverse groove between the process and the articular surface of glenoid (Figs. 5, 9). In *T. grangeri*, the postglenoid process is transversely shorter and lacks the distinct lateral rim and transverse groove between it and the fossa (Fig. 10).

Auditory Region (Petrosal)—Gazin (1953) mentioned that tillodonts do not have osseous tympanic bullae. Except for

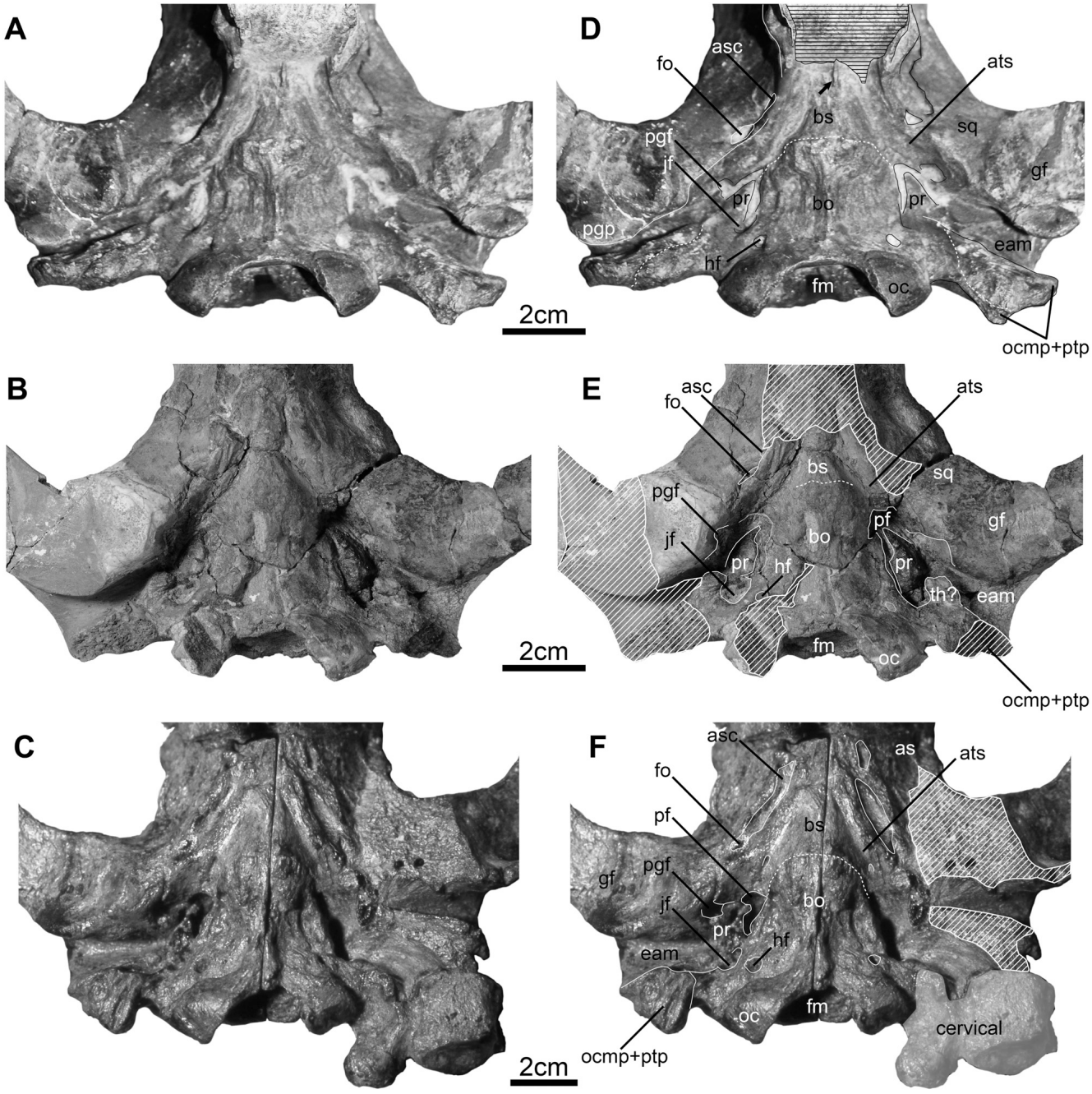

FIGURE 10. Basicrania of trogosine tillodonts in ventral views. **A–C**, unlabeled; **D–F**, labeled with anatomical abbreviations used in text. **A, D** *Trogosus grangeri* (AMNH 17008, holotype); **B, E**, *T. hillsii* (USNM 17157, holotype); **C, F**, *Tillodon fodiens* (YPM 11087, holotype). Arrow in **D** indicates midline crest (keel) of basisphenoid. White and black hatching indicate breakage and matrix in the choanae, respectively.

Gazin's brief comments on petrosals of *Trogosus* and *Tillodon*, the tillodont auditory region has not been described in detail nor figured. No tillodont fossils preserving a complete auditory region have been reported previously. However, SDSNH 40819 preserves a complete auditory region on the left side and a nearly complete one on the right side (Figs. 9, 11).

Gazin (1953) emphasized the short basicranium as a distinct feature of trogosine tillodonts, and he presumed a "prominent anteroposteriorly compressed process" (named "occipitomastoid process" in Gazin, 1953:56) lateral to the occipital condyle to be a complex consisting of mastoid, exoccipital (paracondylar process), and postympanic process of squamosal. Specimen SDSNH 40819 clearly demonstrates that the process is composed of the mastoid process of the petrosal (anterolateral half) and the paracondylar process of the exoccipital (posteromedial half) (occipitomastoid process in Figs. 5, 6, 9, 10, 12) and laterally contacts with the postympanic process of the squamosal (Figs. 9, 11). Figure 11 illustrates and labels the complex anatomy in and around the auditory region of SDSNH 40819. The homology of these features is based on discussions in Gazin (1953) and additional

studies focused on plesiomorphic petrosal features in other Paleogene mammals (e.g., Cifelli, 1982; Coombs and Coombs, 1982; Geisler and McKenna, 2007; Wible, 2008).

In SDSNH 40819, the medial edge of the right promontorium of the petrosal contacts and is partially underlapped by the lateral margin of the basioccipital, whereas the left promontorium is separated from the basioccipital by a fissure (piriform fenestra) continuous with the jugular foramen (posterior lacerate foramen). Although it appears likely that the right promontorium is in situ and that the left promontorium has been separated during diagenetic deformation, in other basicrania (Fig. 10) a narrow piriform fenestra seems to be present between the anterior half of the promontorium and the basioccipital. Specimen SDSNH 40819 clearly shows the piriform fenestra, with a round anterior margin on either side. The protuberant promontorium displays a defined ventral groove for the stapedial artery (Fig. 11). Posterior to the piriform fenestra, what is likely the anterior part of the promontorium is poorly preserved, suggesting that it was poorly ossified. The posteriomedial border of the jugular foramen is rounded, whereas the anterolateral margin is lobate, with small notches on either side, possibly for the passage of cranial nerves (the 9th, 10th, and 11th nerves, according to Gazin, 1953) (Fig. 11). In *T. grangeri* and *T. hillsii*, the promontorium, although poorly preserved, bears no distinct groove for the stapedial artery. The jugular foramen in *T. hillsii* is apparently larger (Fig. 10).

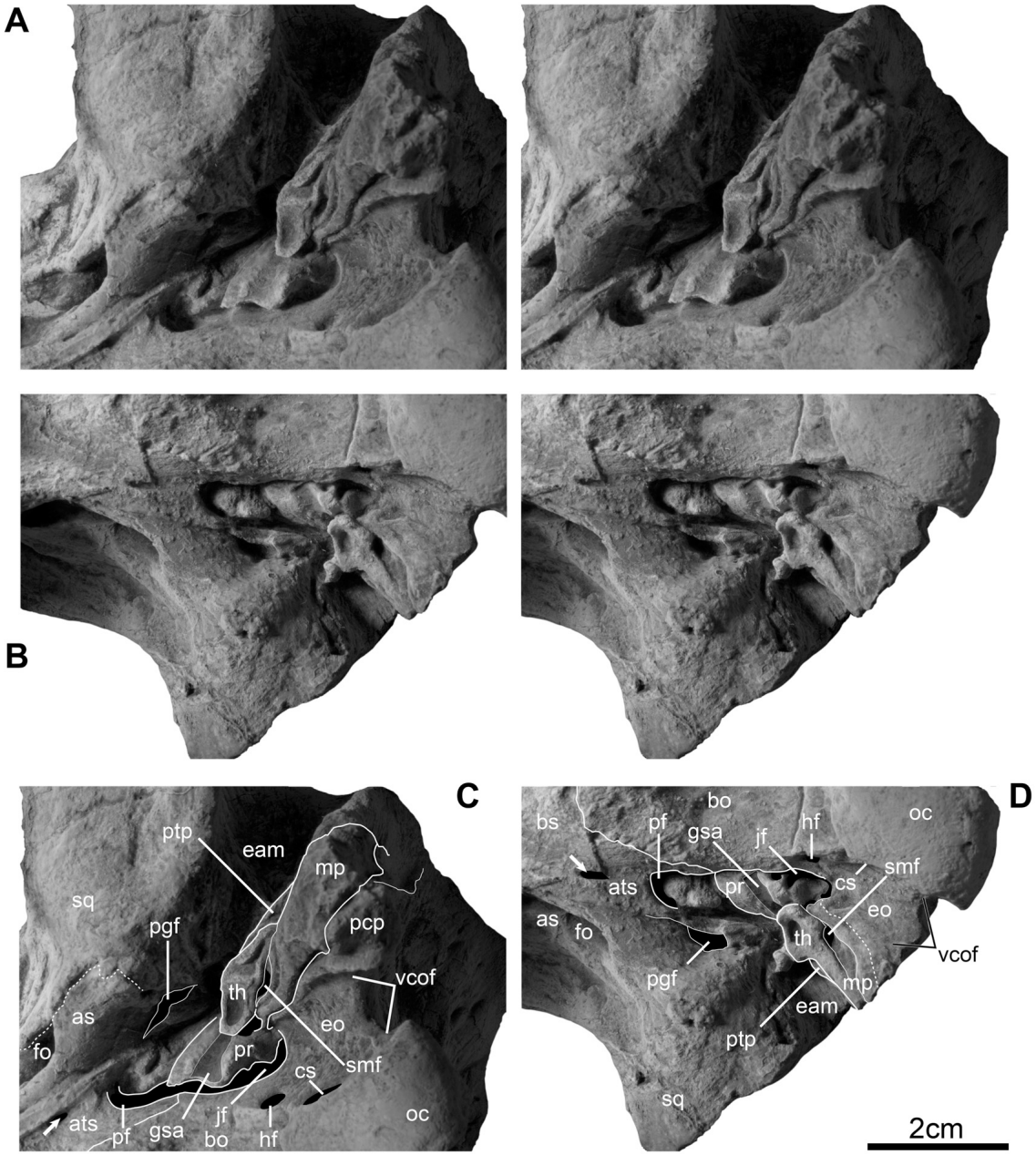

FIGURE 11. Auditory region of referred skull of *Trogosus castoridens* (SDSNH 40819) in ventral views of left (**A, C**) and right (**B, D**) sides, coated with ammonium chloride sublimate. Anterior to the left. **A, B**, stereographs; **C, D**, labeled photographs with anatomical abbreviations used in text. Arrows indicate foramina on the auditory tube sulci.

The occipitomastoid process of SDSNH 40819 is similar to that of *Tillodon fodiens* in being knob-like, and readily differentiated from the more anteroposteriorly compressed processes of *T. grangeri* and *T. hillsii* (Fig. 10; character 69). The occipitomastoid process of SDSNH 40819 is directed posteroventrolaterally (about 60° from the sagittal plane) and descends to a level coincident with the ventral margin of the occipital condyle (Fig. 6). The mastoid process pinches out dorsally between the squamosal (postympanic process) and the exoccipital (paracondylar process) and becomes broader posteroventrally, occupying the anterolateral half of the knob-like head of the occipitomastoid process (Fig. 11). Each contact with the adjacent bones is clearly defined, especially the ventral contact with the exoccipital, which exhibits a narrow groove. The posterolateral edge of the head of the occipitomastoid process is swollen near the contact with the squamosal, whereas the posterior surface of the head is concave along the contact with the exoccipital.

There is a clearly defined tympanohyal in SDSNH 40819 (Figs. 9, 11). It is developed as a flange extending anteromedially beneath the posterior portion of the promontorium. The tympanohyal displays a small and shallow depression on the ventral surface that probably marks the location of the articulation with the stylohyoid. A small fissure-like stylomastoid foramen occurs just medial to the tympanohyal (Fig. 11). These petrosal structures are unfortunately not preserved in other tillodont basicrania.

Occipital—The dorsal and right margins of the occipital forming the nuchal crest and the right paracondylar process of the exoccipital are missing in SDSNH 40819. The preserved occipital forms a weakly concave occipital shield with a roughly fan-shaped outline in posterior view. Unfortunately, the delimitation between individual occipital components (e.g., supraoccipital and exoccipital) has been obliterated by sutural fusion. The sutures with the parietal and squamosal around the nuchal crest are also indiscernible, although the left occipital preserves faint, traceable sutures with the adjacent squamosal and the mastoid process of the petrosal behind the lateral nuchal crest (Figs. 11, 12).

Like in *T. hillsii*, occipital height in SDSNH 40819 is two-thirds of occipital height in *T. grangeri* (Figs. 6, 7, Table 1). The dorsal half (supraoccipital) of the occipital shield, although slightly deformed, projects posteriorly to overhang the occipital condyles and exoccipital (Fig. 6). In posterior view, at least three visible anteroventromedially directed vascular foramina (supraoccipital foramina) are present on the left supraoccipital (Fig. 12). The occipital shield is depressed above each occipital condyle, and the central part of the shield is marked by a low eminence medially extending from the dorsal side of each condyle (character 70 [0]). The preserved left exoccipital surface bears a well-defined, vertically oriented crest (exoccipital crest in Fig. 12), which is dorsally continuous from its contact with the mastoid process of the petrosal.

The aperture of the foramen magnum is ovoid in SDSNH 40819. Each occipital condyle has a posteroventrally rounded facet and faces posterodorsolaterally. The distance between the condyles is wider dorsally than ventrally and becomes narrower anteriorly (Figs. 9, 12). The anterior-most distance between the condyles is as narrow as the transverse width of one condylar facet. The odontoid notch is relatively narrow (Fig. 9; character 71[1]). The dorsomedial surface of each occipital condyle bears a small aperture, the dorsal condyloid foramen (Fig. 12), which potentially continues to the hypoglossal foramen.

In ventral view, the paracondylar process of the exoccipital (= posteromedial part of occipitomastoid process) bears a crest-like eminence along the contact with the mastoid process. The occipitomastoid process is separated from the occipital condyle by a narrow, saddle-like depression, the ventral condyloid fossa (Fig. 11). This fossa continues anteriorly into the trough-shaped channel that enters the jugular foramen. On the medial surface of this channel, there are two small apertures: the anterior one

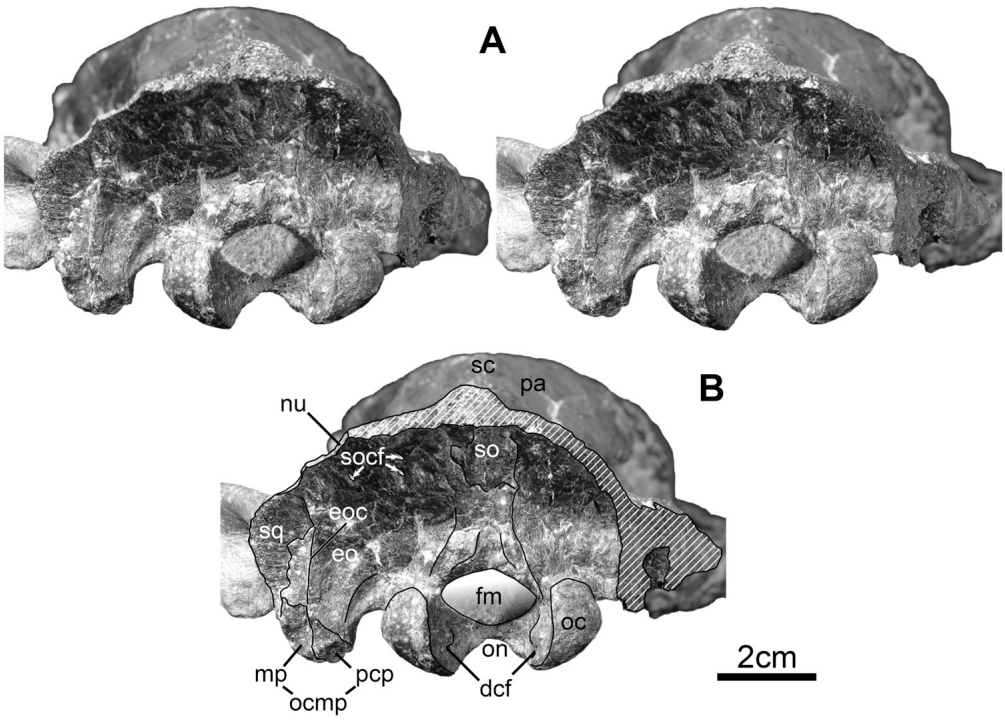

FIGURE 12. Occiput of referred skull of *Trogosus castoridens* (SDSNH 40819) in posterior view. **A**, stereograph; **B**, labeled photograph with anatomical abbreviations used in text. White hatching indicates breakage.

medial to the jugular foramen is the hypoglossal foramen (Figs. 8, 11), whereas the posterior one near the anterior border of the condyle is here designated the 'condyloid sinus' (Figs. 8, 11).

The ventral surface of the basioccipital in SDSNH 40819 has a roughly quadratic outline, formed by the parasagittal medial edges extending anteriorly from the ventral condyloid fossae to a subrectangular contact with the basisphenoid (Fig. 9; character 72[0]). A weak keel is present along the midline of the basioccipital. The lateral sides of this keel exhibit a shallow ovoid fossa (Fig. 9). The contact with the basisphenoid is marked by a faint suture bearing diminutive tuberosities, which probably mark the attachment of the rectus capitus lateralis muscle.

In contrast to the condition in SDSNH 40819, *T. grangeri* has a more flattened occipital shield with weaker exoccipital crests and no distinct dorsal condyloid fossa (character 70 [1]). The occipital shield of *T. hillsii* resembles that of SDSNH 40819. The occipital condyle of *T. grangeri* is almost the same size as that of SDSNH 40819, but is more laterally facing (i.e., anteroposteriorly compressed; character 71[0]). As a result, the ventral condyloid fossa is narrower than that of SDSNH 40819. The foramen magnum in *T. grangeri* is transversely expanded, being roughly 1.5 times the size of that in SDSNH 40819. The foramen magnum is more elliptical in posterior view in both *T. grangeri* and *T. hillsii*, with a triangular midline depression on the dorsal margin. The basioccipital of *T. grangeri* shows wider, ventrolaterally facing surfaces (i.e., 'V'-shaped bottom in coronal plane), with a well-defined midline keel (character 72[1]). In addition, the anterior contact with the basisphenoid is more pronounced. In *T. grangeri* and *T. hillsii*, the condyloid sinus does not appear to be present. Especially in *T. grangeri*, the anteroposteriorly compressed occipitomastoid process is expanded laterally. *Trogosus hillsii* and *Tillodon fodiens* also have laterally facing occipital condyles, with very narrow ventral condyloid fossae and no trough-shaped channel extending to the jugular foramen. The latter condition is also seen in *T. grangeri* (Fig. 10).

Hyoid—Two broken elements possibly representing the right and left stylohyals were preserved with the skull of SDSNH 40819 (Fig. 13). One of these elements, here identified as the partial left stylohyal, was found in matrix inside the left zygoma of the skull. The morphology of tillodont hyoids is poorly known, and the only previous descriptions are those of Gazin (1953), who briefly commented on the incomplete hyoid bones of the holotype (AMNH 17008) of *T. grangeri* (identified as stylohyal and epihyal). Identification of the hyoid elements described here is based on comparison with the hyoids of *T. grangeri*. The correctness of this identification should be reevaluated when additional tillodont hyoids are discovered.

The right and left stylohyals in SDSNH 40819 lack the proximal-most process and half of the shaft, respectively. Figure 13 illustrates the probable outline inferred for each element. The stylohyoid is bifurcated into the rostral shaft and downwardly extending stylohyal angle. These branches are slightly thinner and broader than in *T. grangeri*. However, as in the latter taxon, the branches appear to face medially as they extend away from the bifurcation. The tympanohyal process is shorter in SDSNH 40819, although the angle of bifurcation is slightly broader than in *T. grangeri*. The dorsal extremity of the tympanohyal process in SDSNH 40819 is rectangular with a slight concavity, but the facet for the basicranial contact is unclear because of poor preservation. The rostral shaft of the stylohyoid is slightly longer than the stylohyal angle and bears a rounded extremity that contacts the epihyal. The lateral surface from the shaft to the tympanohyal process shows a very faint groove, whereas the medial surface is slightly convex. These features are not seen in *T. grangeri*.

Upper Dentition

The upper dentition of SDSNH 40819 is relatively well preserved (Fig. 14), except for breakage of the labial portions of the right molars. In addition, the right and left P2s are missing, as is the left I3. The right I3 and left C1, although present, have become separated from the skull. All preserved cheek teeth are lightly worn.

The distance between the posterior margin of I2 and the anterior margin of P2 (i.e., I2–P2 distance) is absolutely and

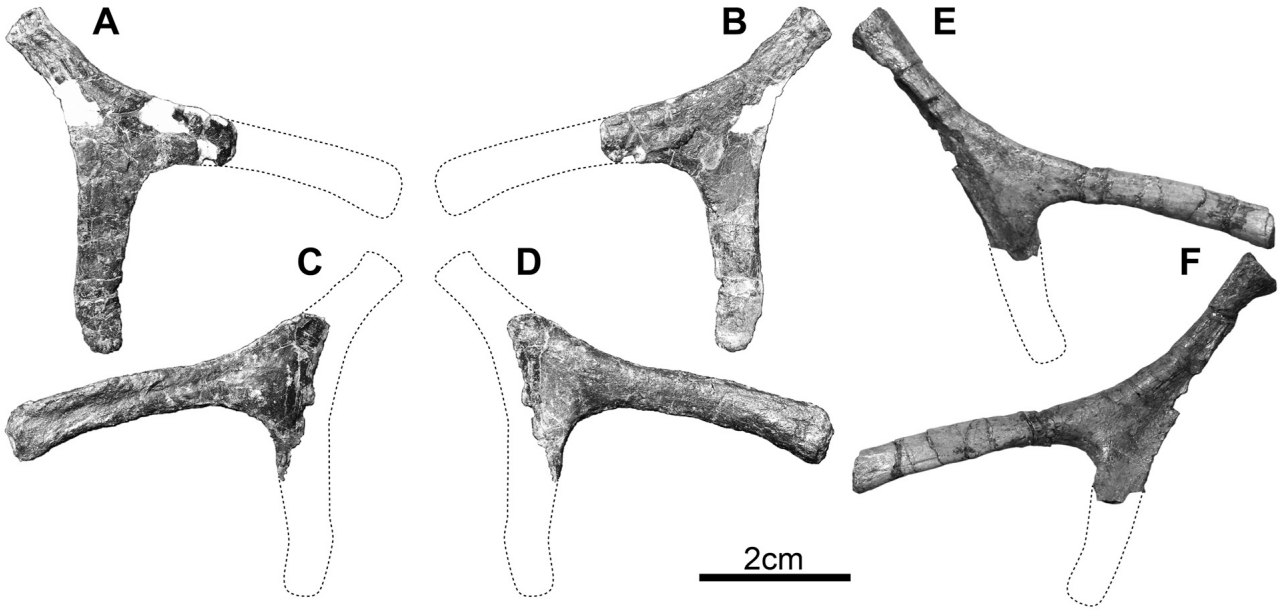

FIGURE 13. Referred stylohyals of *Trogosus castoridens* (SDSNH 40819), right (**A, B**) and left (**C, D**) and *Trogosus grangeri* (AMNH 17008, holotype), right (**E, F**). **A, C, E**, outer and **B, D, F**, inner views.

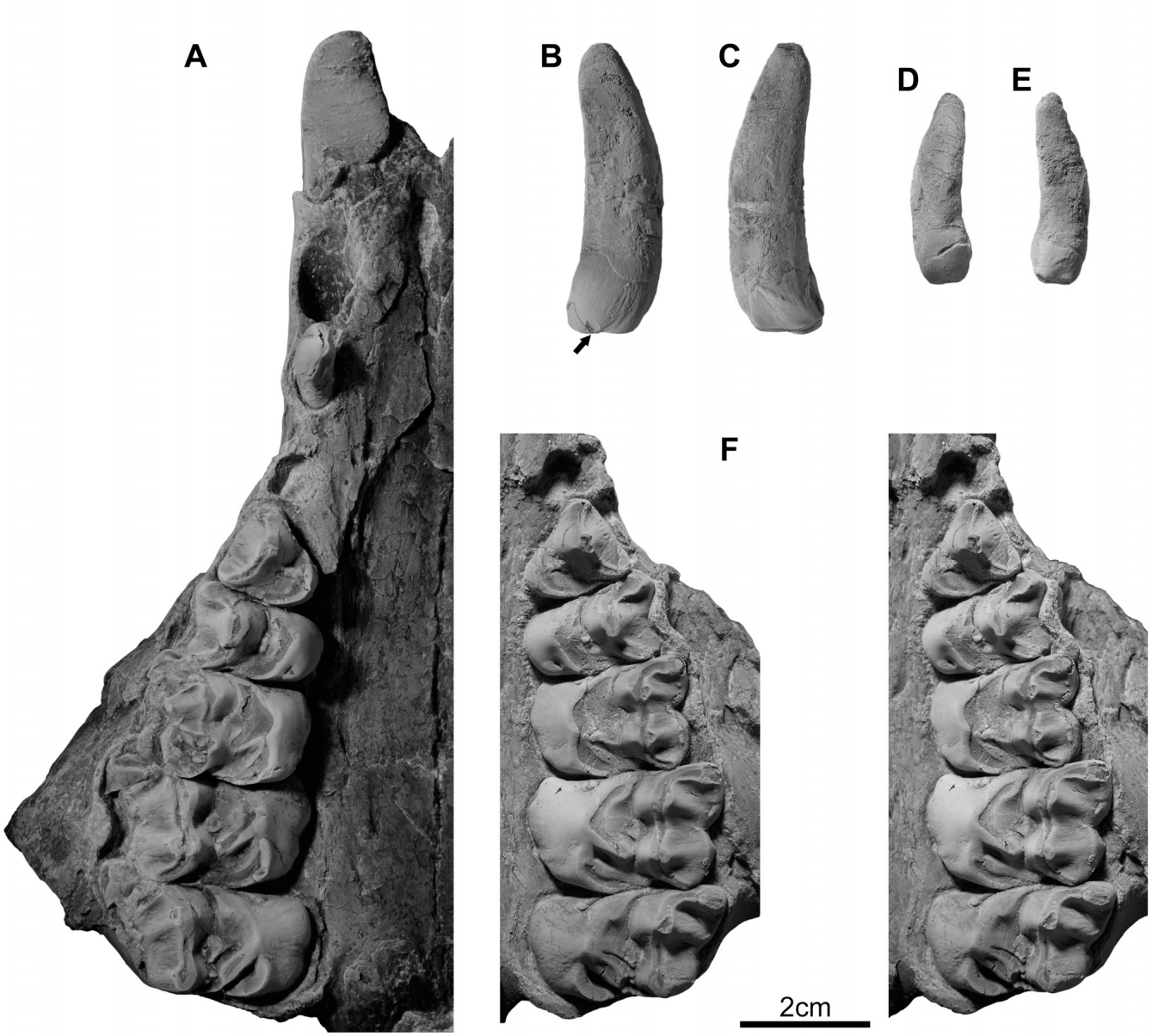

FIGURE 14. Upper cheek teeth of referred skull of *Trogosus castoridens* (SDSNH 40819), coated with ammonium chloride sublimate. **A**, right upper tooth series (I2–M3), occlusal view; **B, C**, right I3, labial and lingual views; **D, E**, left C1, labial and lingual views; **F**, stereograph of left P3–M3, occlusal view. Arrow indicates a small wear facet on the labial side of I3 crown.

proportionately shorter than in other species of *Trogosus* (Fig. 14, Table 1; character 20[1]) and serves as a metric for differentiating between 'short-faced' *Trogosus* (*T. castoridens*) and 'long-faced' *Trogosus* (*T. hyracoides* and *T. grangeri*). However, in the same individuals of trogosine tillodonts, the I2–P2 distance is about 60–80% longer than the i2–p3 distance (Table 1). It is noteworthy that the I2–P2 distance in SDSNH 40819 (average 40.7 mm) is nearly twice as long as that of the i2–p3 distance in the holotype (ANSP 10337) of *T. castoridens* (19.0 mm; Table 1).

In the lower dentition, the p2–p3 diastema is longer than any of the other diastemata anterior to p3, and may thus be useful as an index for assessing the degree of anterior elongation of the rostrum when making comparisons with incomplete specimens (Miyata, 2007a). In the upper dentition, the length of the C1–P2 diastema may also serve as a useful index of rostral elongation. However, in *T. hillsii*, the I3–C1 diastema is longer (ca. 7.2 mm) than the C1–P2 diastema (3.2 mm), unlike in other *Trogosus*, which suggests that we should pay attention when comparing with incomplete material showing an upper anterior diastema.

Incisors and Canines—The enamel of the right I2 and the tip of the left I2 in SDSNH 40819 is slightly damaged. Both I2s, however, preserve the characteristic morphology of I2s in *Trogosus*, except for being slightly smaller (Table S2). The I2s are rootless with chisel-shaped tips and have a continuously curved longitudinal profile in lateral view (Fig. 6). The enamel covering of the I2 is ordinary and extends over the anteromesial, labial, and greater part of the distal (lateral) surfaces. The I2 is roughly 'D'-shaped in cross-section at the level of the alveolus, with a rounded labial side and a weakly acute labiomesial corner. The enamel-free dentine portion of the crown is posterodistally expanded. The posteromesial

side of the exposed dentine is marked by a shallow longitudinal groove, which extends along the long axis of I2 (Fig. 14A).

The isolated right I3 of SDSNH 40819 is nearly complete, with a closed pulp cavity and curved, elongate root (Fig. 14B, C). The enamel covering extends further on the labial surface than on the lingual surface, and the crown becomes narrower at the anterior (mesial) and posterior (distal) edges. The posterior half of the crown swells labiolaterally, with a bluntly worn, posteriorly placed, conical cusp. A prominent vertical crista forms the posterolabial corner of the crown and intersects the posterior cusp. A distinct wear facet extends across the entire occlusal surface of the crown and likely reflects heavy occlusion with the chisel-like i2. Besides the major occlusal wear facet, there is a small, oval wear facet on the labial side of the I3 crown, close to the edge of the occlusal surface (arrow in Fig. 14B). This minor wear facet likely is the result of incidental occlusion with the tip of the i2, and not with a small tooth posterior to i2, such as i3 or c1. The I3 of SDSNH 40819 is similar to that of *T. grangeri* (AMNH 17008) in size and morphology (Table S2; see also measurements in Gazin, 1953), except for having a slightly longer root in the former. The I3 of *T. hyracoides* (USNM 17886) has a much broader labial enamel distribution, which extends into the alveolus.

The isolated left C1 is small, with an elongate, closed root that curves posteriorly in lateral view (Fig. 14A, D, E). The crown of both canines is labiolingually compressed and possesses a small, bluntly worn and centrally placed cusp. The anterior edge of the crown is stouter than the posterior one, which displays a short, vertical crista. The apex of the tooth bears a distinct wear facet that extends across the entire occlusal surface of the crown and is likely the result of occlusion with the posterior wall of c1. The enamel extends farther up the labial side of the crown than the lingual side. No significant differences in C1 size and morphology can be observed between SDSNH 40819 and *T. hyracoides* (USNM 17886), the only other species of *Trogosus* for which a well-preserved C1 is known.

Premolars—On each side, SDSNH 40819 preserves the alveolus for a single-rooted P2 that is almost equal in size to the C1 alveolus (Fig. 14A). The crowns of both the right and left P3s and P4s are intact and probably represent the least worn and best-preserved examples of trogosine premolar morphology.

The crown outline of P3 in SDSNH 40819 is almost triangular in occlusal view, as also seen in other species of *Trogosus* (Miyata, 2007b). The P3 paracone is high and conical, being positioned in the middle (left P3) or slightly anterior to the middle (right P3) of the labial crown (character 3[0]). The labial enamel extends to the root. There is a weak wear facet extending from the anterior edge of the paracone to the parastyle (Fig. 14A, F). The P3 parastyle of SDSNH 40819 is smaller than in *T. hyracoides*, but is rather similar to that of *T. hillsii* in being a crest-like, defined cusp separate from the paracone (character 2[0]). The crest-like metastyle of P3 is expanded posterolabially with an acute corner (character 4[1]) and joined to the paracone by a low ridge (ectoloph). The lingual half of the P3 is dominated by the protocone shelf. The protocone is connected to the anterolingual side of the paracone by a faint enamel ridge, and to the metastyle by a narrow postprotocrista. A diminutive enamel ridge extending from the protocone is present at the lingual enamel base of the paracone, and a faint anterior cingulum is present on the anterior corner of the paracone. The P3 of SDSNH 40819 is similar to that of *T. hillsii* in having an almost mid-positioned (intermediate) paracone and reduced anterior cingulum, but differs from that of *T. hyracoides*, which bears a much higher paracone, a sharp anterior cingulum, and a larger parastyle. The P3 of SDSNH 40819 is distinct from those of *T. gazini* and *T. latidens* in having a mid-positioned paracone and crest-like parastyle (see also Miyata, 2007b).

The P4 paracone is a prominent cusp positioned almost in the middle of the ectoloph (Fig. 14A, F). The P4 parastyle and metastyle are equally expanded labially, and the former has a slightly rounded corner. The crown is weakly compressed anteroposteriorly on the labial side, with a narrow ectoflexus, unlike the condition in *T. hyracoides* and *T. grangeri*. The preprotocrista extends anterolabially from the protocone and continues to the anterior cingulum connecting to the parastyle, whereas the postprotocrista is expanded posterolingually and links to the posterior wall of the metastyle. These crests from the protocone form a slightly asymmetric V in occlusal view (Fig. 14A, F; character 7 [1]). There are diminutive enamel beads on the notch between the paracone and postprotocrista. A small enamel swelling with a diminutive sinus (possibly homologous with the well-developed hypocone on the molars; see Miyata, 2007b) is present just posterior to the protocone (character 8[1]). The P4 of SDSNH 40819 is similar to that of *T. hyracoides* in being less asymmetrical, with an almost mid-positioned paracone in occlusal view, but the paracone is much lower than in the latter species. The P4 of SDSNH 40819 is differentiated from the more asymmetric P4s of *T. gazini* and *Tillodon latidens*, which have more reduced preprotocristae and anteriorly swelling lingual walls (Miyata, 2007b).

Molars—The left molars are slightly better preserved than the right ones in SDSNH 40819 (Fig. 14). General molar structure in this specimen does not differ significantly from that of other *Trogosus* except for being more brachydont, with expanded and gently sloping lingual walls like in *T. hillsii* and *T. gazini* (see also Miyata, 2007b). Minor differences mentioned below are recognized, but some of these features potentially may fall within the range of intraspecific variation. The labiolingual width of the molars increases from M1 to M3, but the M3 is slightly shorter anteroposteriorly than the M2 (Table S2; character 11[0]). The metastyles on M1 and M2 are slightly better developed than in *T. gazini*. The hypocone crest on each molar is moderately expanded posteriorly, especially in M2. The labial cingula on M1 and M2 are reduced and discontinuous. The precingulum anterior to the protocone is vestigial on both M1 and M2, but is more distinct on M3. The M3 postprotocrista extends posteriolabially and connects to the cingulum on the posterior side of the metacone, as in *T. hyracoides*. In *T. gazini* and *T. latidens*, the M3 has no such cingulum on the posterior surface (Miyata, 2007b).

Dentary

The right and left dentaries of SDSNH 40819 are incomplete and consist only of the proximal half of the horizontal ramus behind the m2, as well as the ascending ramus. In each dentary, the posteroventral extremity of the angular process is missing. The right dentary is more complete than the left and preserves both the condylar and coronoid processes (Fig. 15).

Overall, the horizontal ramus of SDSNH 40819 is shallower and more slender than in *T. hyracoides* and *T. grangeri* (Table 1; character 29[1]). Labiolingually, the ramus at the level of m2 is narrow, as also seen in the holotype of *T. castoridens* (ANSP 10337). The anterior margin of the ascending ramus forms an angle of approximately 60° with the tooth row (Fig. 15). Its origin is just behind the m3 talonid, as in *T. hillsii*, whereas in other trogosine species there is a short space between the m3 and the anterior root of the ascending ramus. The masseteric fossa extends anteriorly to a level below the m3 talonid and is shallower than those of *T. hyracoides* and *T. grangeri*. The coronoid process is slightly lower than in *T. grangeri*, whereas the condylar process is moderately stout. The articular surface of the condylar

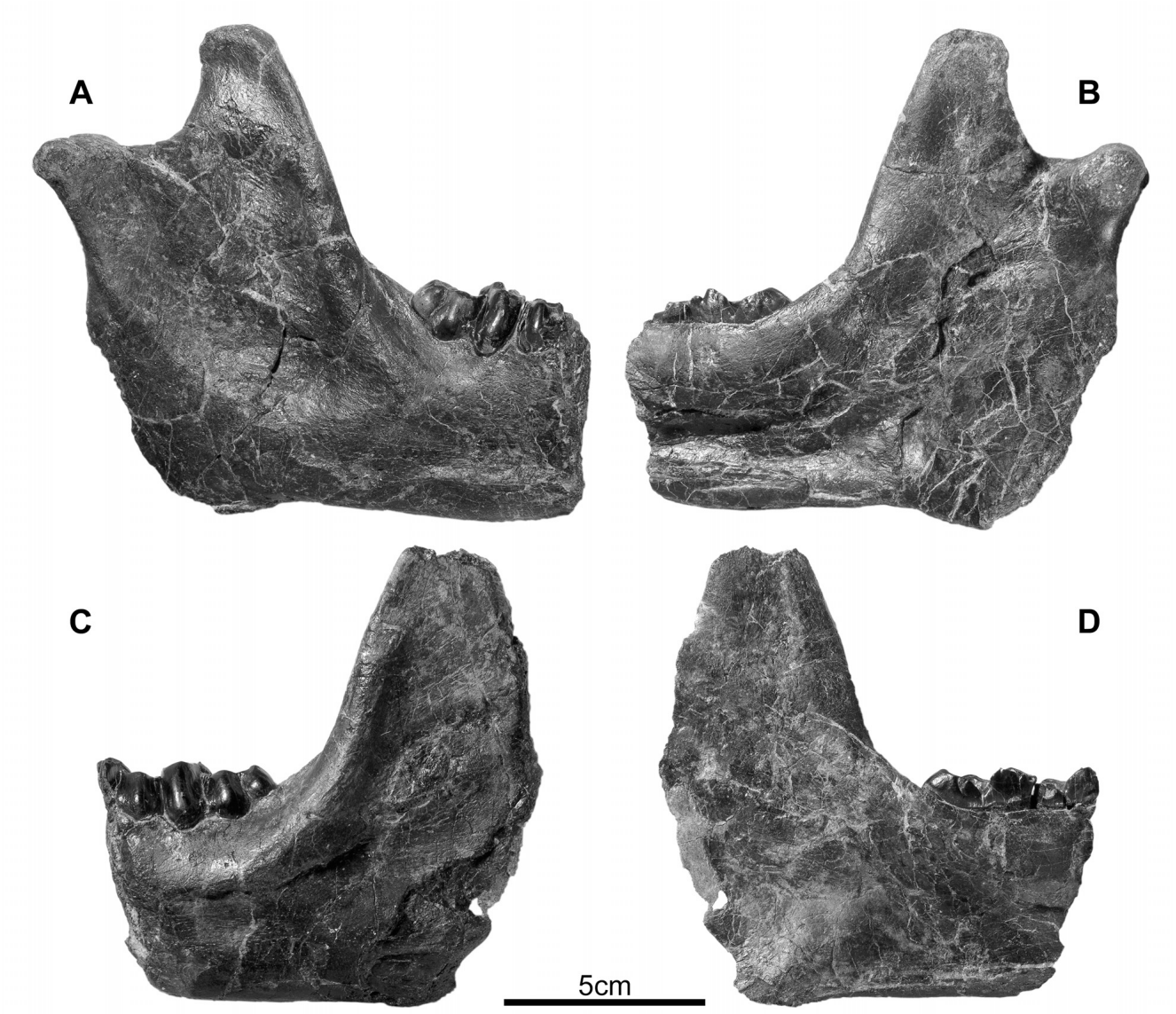

FIGURE 15. Posterior portions of dentaries of referred skull of *Trogosus castoridens* (SDSNH 40819), right (**A, B**) and left (**C, D**). **A, C**, labial and **B, D**, lingual views.

process is dorsally placed and elevated well above the m3 crown (ca. 35 mm). Although the distal portion of the angular process is missing in SDSNH 40819, the transverse thinness of the ramus suggests that the process was not as large as in *T. hyracoides* and *T. grangeri*.

Lower Dentition (Molars)

As is the general pattern in species of *Trogosus*, the lower molars of SDSNH 40819 have relatively low crowns, columnar labial walls of the trigonid and talonid, flattened lingual walls, and cristid obliquae connecting with the posterolingual walls of the trigonids (Fig. 16). Although SDSNH 40819 is comparable in molar size to the holotype (ANSP 10337) (Table S2; see also Miyata, 2007a), the molar cusp pattern of the holotype cannot be compared because of breakage. The left m2 in SDSNH 40819 is more complete than the right and preserves the posterior part of the trigonid and a weak metastylid. The hypoconulid-entoconid basin (the second basin) is likely not present on the m2 talonid (character 25[1]). The hypoconulid and entoconid cannot be distinguished because of wear, but form a narrow crest continuous from the posterior end to the posterolingual corner of the talonid (Fig. 16A, D).

Both m3s are present in SDSNH 40819 and become narrower posteriorly (Fig. 16). There is no visible precingulid. The m3 trigonid is less tapering upward and lacks the flattened posterolabial wall (postprotocristid) with wear facets seen in *T. gazini* (Miyata, 2007b). The metastylid protrudes from the metacone posteriorly, but is rather weak (character 26[0]). The m3 hypoconulid forms the bulbous third lobe (hypoconulid lobe; Fig. 16). The entoconid on each side is crest-like, but the right one bears two faint, step-like enamel protuberances on the anterior slope. No hint of a posthypocristid is seen on the m3 third lobe, although the occlusal detail of the third lobe basin is obscure due to wear. If present, the posthypocristid is much weaker than or comparable to that of *T. hyracoides* (character 27; see also Miyata, 2007b). A very narrow but distinct groove extends

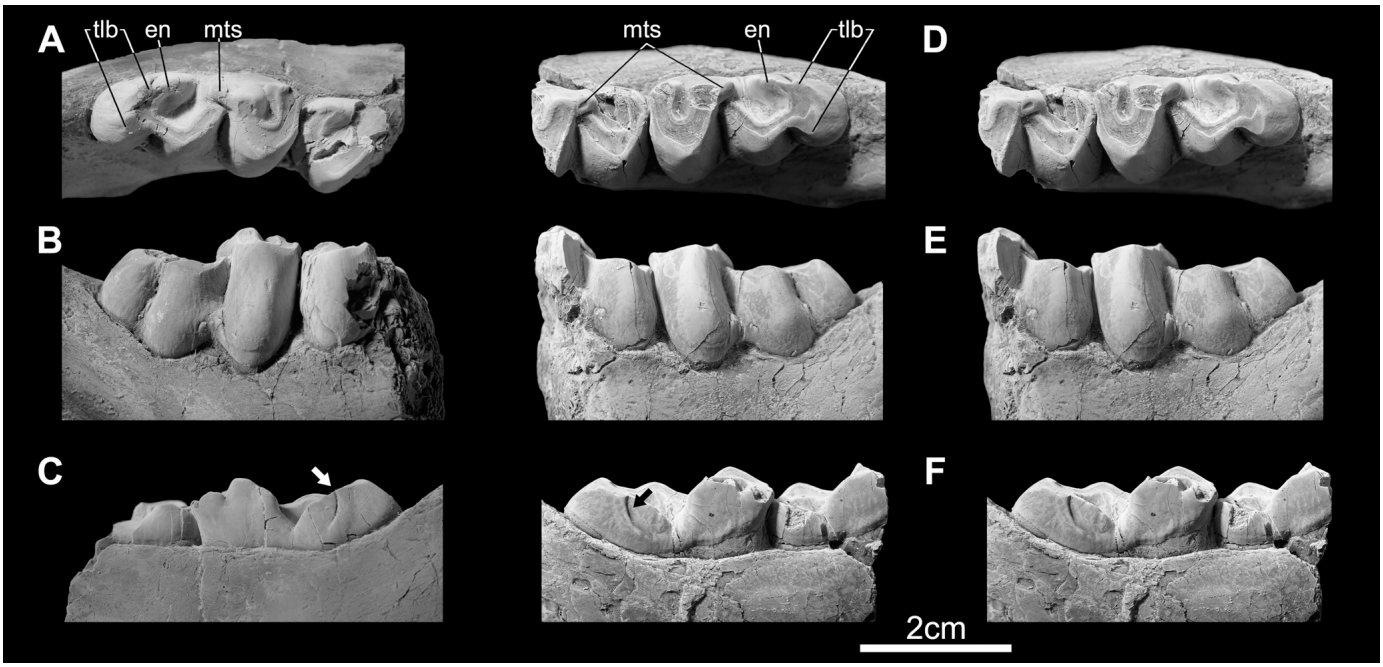

FIGURE 16. Lower molars of referred dentaries of *Trogosus castoridens* (SDSNH 40819), right (**A**–**C**) and left (**D**–**F**, stereographs) in occlusal (**A, D**), labial (**B, E**), and lingual (**C, F**) views. All are coated with ammonium chloride sublimate. The m2s on both dentaries are incomplete. Arrow indicates the lingual extension of the groove between the hypoconulid and entoconid on m3. **Abbreviations**: **en**, entoconid; **mts**, metastylid; **tlb**, third lobe basin (= hypoconulid).

posterodorsally on the lingual enamel surface of the third lobe (arrows in Fig. 16C, F; character 28[1]). This groove appears to be the lingual extension of the groove separating the third lobe (hypoconulid) and entoconid, but is unknown in previously described *Trogosus* dentitions. The lingual talonid notch between the metastylid and entocristid is somewhat narrower than in *T. gazini*.

Cervical Vertebrae

Atlas—The atlas of SDSNH 40819 is nearly complete, missing only the anterolateral corner of the right transverse process (Fig. 17A–D). It is relatively short anteroposteriorly, and the anterior articular surfaces for the occipital condyles are deeply concave. Each posterior articular surface for the axis is weakly concave and nearly circular. The transverse process on each side is relatively short with a flabellate lateral margin (character 73 [0]). In anterior view, the transverse processes are slightly concave dorsally. A relatively small transverse foramen penetrates the base of the transverse process immediately adjacent to the centrum (Fig. 17A, Table S3). A foramen for the first spinal nerve is present at the base of the dorsal arch and is transversely oriented. A low, knob-like neural spine is present near the middle of the dorsal arch (Fig. 17A, C; character 74[1]).

There are only two previously described trogosine atlas vertebrae: a complete atlas of *T. grangeri* (AMNH 17008, holotype; Fig. 17E, F) and an incomplete (right half) atlas of *Trogosus* cf. *T. latidens* from Japan (see Miyata, 2007a). The atlas of SDSNH 40819 is distinct from that of *T. grangeri* in being dorsoventrally shorter and having laterally shorter transverse processes (Table S3). The atlas of *T. grangeri* is stouter with more posterodorsally expanded transverse

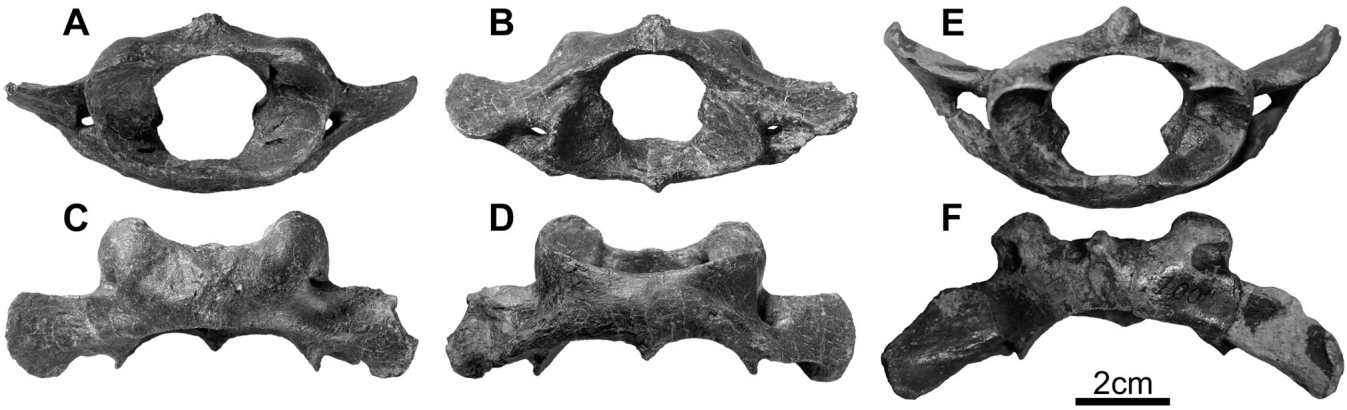

FIGURE 17. Referred atlas of *Trogosus castoridens* (SDSNH 40819) (**A**–**D**) compared with that of *Trogosus grangeri* (AMNH 17008, holotype) (**E, F**). **A, E**, anterior; **B**, posterior; **C, F**, dorsal; **D**, ventral views. Anterior at top in dorsal and ventral views.

processes, more robust bases of the transverse processes, and larger transverse foramina (Fig. 17E, F, Table S3). Moreover, the spine on the dorsal arch is more anteriorly located in *T. grangeri* (character 74[0]). The atlas of SDSNH 40819 is more slender compared with that of *Trogosus* cf. *T. latidens* from Japan. The distance between the articular facets for the axis in SDSNH 40819 is greater than it is in *T. gazini* (USNM 364762, holotype; see Miyata, 2007b), although the latter is slightly compressed laterally. The general form of SDSNH 40819, with its shorter transverse processes, resembles that of the primitive tillodont *Azygonyx* (UM 68511, holotype of *A. ancylion*). However, the sulcus dorsal to the articular facet for the axis is more distinct in *Azygonyx* (character 75[0]).

Other Cervical Vertebrae—Three associated cervical vertebrae were preserved separately in the same sandstone block, and after mechanical preparation they can be articulated (Fig. 18). The three cervicals are identified here as the fifth to seventh, as described below, although a comparable cervical series in *Trogosus* has not been reported previously. Gazin (1953) noted that USNM 17886 (*T. hyracoides*) includes remains from the fourth cervical to the first dorsal, but the materials are too poorly preserved to serve as the basis for a proper comparison. Additional cervical vertebrae of other trogosines are known, but they are also poorly preserved (see below).

The anterior cervical (the fifth) of SDSNH 40819 is apparently shorter anteroposteriorly, compared with the possible third cervical of AMNH 17011 (*Trogosus* sp. from the Huerfano Basin, Colorado; Gazin, 1953), the possible fourth cervical of *Trogosus* cf. *T. latidens* from Japan (see Miyata, 2007a), and the third cervical of *Tillodon fodiens* (USNM 18164; Gazin, 1953). The cervicals of SDSNH 40819 become progressively shorter posteriorly (Fig. 18E, F, Table S3). Each centrum is transversely expanded and dorsoventrally compressed (Fig. 18). The anterior articular surface on each centrum faces slightly anteroventrally; thus, each posterior surface faces posterodorsally. The fifth cervical has a stout, high neural spine projecting posterodorsally, whereas that of the seventh cervical is thinner and more vertically directed. The transverse process of the fifth cervical is short, with a weak keel on its ventral edge, and the processes of the sixth and seventh cervicals are longer and stouter, with keels developed on their anterior and lateral margins. The transverse foramen is circular on the fifth cervical, and oval on the sixth and seventh cervicals. Each zygapophysis is strong, with a flattened and oval articular facet. In lateral view, the fifth cervical has the prezygapophysis lower than the level of the postzygapophysis, whereas on the sixth cervical they are almost at the same level and on the seventh cervical the prezygapophysis is located slightly higher than the postzygapophysis. Together, these features of the centra and zygapophyses suggest that, when articulated, the cervical series had a slight anterodorsal orientation (Fig. 18E). In the seventh cervical, a pair of small concavities on the posteromedial bases of the prezygapophyses fits the postzygapophyses of the sixth cervical (Fig. 18C, F). The seventh cervical, in addition, bears a pair of short accessory processes on the dorsal arch, medial to the postzygapophysis (Fig. 18C, D), which likely articulated with the metapophysis of the first dorsal vertebra.

PHYLOGENETIC ANALYSIS

Prior to assignment of SDSNH 40819 to *Trogosus castoridens*, this taxon was known only from the holotype specimen (ANSP 10337), an incomplete mandible with fused dentaries bearing poorly preserved (heavily worn and/or broken) cheek teeth (Gazin, 1953). As a consequence, *T. castoridens* was primarily diagnosed as a short-faced *Trogosus* species possessing a shallow dentary with a relatively short distance between i2 and p3, and possibly the loss or reduction of i3 (Gazin, 1953; characters 17[1] and 20[1] in Miyata, 2007b). Specimen SDSNH 40819 does not preserve directly comparable parts with the holotype, except for the posterior part of the dentaries and the m2–m3 series. Referral of SDSNH 40819 to *T. castoridens* is largely based on the comparable shallow horizontal ramus and short dentary (inferred from the skull), and not on any dental characters because of the poor preservation of the holotype dentition. Although this may appear to be limited morphological evidence to support assignment of SDSNH 40819 to *T. castoridens*, the results of our phylogenetic analysis as presented below, together with our current understanding of the taxonomy of nominal *Trogosus* species, suggest that this is the most parsimonious taxonomic hypothesis.

Methods

Miyata (2007b) examined trogosine phylogenetic relationships by conducting a parsimony analysis using PAUP* 4.0b10 (Swofford, 2003), based on a character-taxon matrix composed of 12 taxa (including two outgroups) and 31 characters (27 dental and four dentary characters). Although Asian trogosines, except *Kuanchuanius shantunensis*, were not included in the analysis owing to their incompleteness, the most parsimonious trees obtained by Miyata (2007b) supported a monophyletic trogosine group with the basal position occupied by *K. shantunensis*. Support for the internal nodes in the resulting trees was weak, and *Trogosus* as a group was found to be paraphyletic, with *Tillodon fodiens* positioned as a terminal taxon within a clade composed of *Trogosus gazini* and *Trogosus latidens*.

To evaluate the taxonomic and phylogenetic relationships of SDSNH 40819, we added 44 new characters to the character-taxon matrix of Miyata (2007b) and conducted a parsimony analysis using PAUP (in total, 75 characters and 12 taxa plus SDSNH 40819; see Supplementary Data). A total of 31 characters (characters 1–27, 29–32 in this paper) and their character coding follow Miyata (2007b). The descriptions of the 44 new characters (characters 28, m3 talonid; 33–72, cranial; 73–75, atlas) and their character coding are summarized in Appendices S1 and S2 of Supplementary Data, respectively. All characters were treated as equally weighted and unordered. The cranial characters of outgroup taxa (*Azygonyx* and *Esthonyx*) were scored based on examination of USNM 18202 (*Esthonyx acutidens*; see Gazin, 1953) and the cast of UM 68511 (holotype of *Azygonyx ancylion*; see Gingerich and Gunnell, 1979). The cranial morphology of these stem tillodonts, however, has not been described in detail in previous studies. The present study is focused on resolving phylogenetic relationships within trogosine tillodonts; consequently, our character-taxon matrix might not include all characters that would likely be plesiomorphic at the level of Trogosinae.

As noted above, the characters shared by SDSNH 40819 and ANSP 10337 are limited (characters 20[1] and 21[1]), except for a few additional synapomorphies that are found in all North American trogosines (characters 15[1], 29[1], 32[1] = 15[1], 28 [1], 31[1] in Miyata, 2007b). In order to assess the relationships of SDSNH 40819 to other trogosines and to test competing hypotheses (Does SDSNH 40819 represent a new species, a specimen of *T. castoridens*, or a specimen of another named trogosine species?), a series of separate analyses of the data were performed.

To test the hypothesis that SDSNH 40819 represents a new species, we conducted analyses with SDSNH 40819 and ANSP 10337 as separate operational taxonomic units (OTUs). Because the holotype of *T. castoridens* (ANSP 10337) is so fragmentary, we ran two analyses of the data, the first using only dental and dentary characters (characters 1–32) (Miyata, 2007b) and the second using all characters (characters 1–75). A heuristic and an

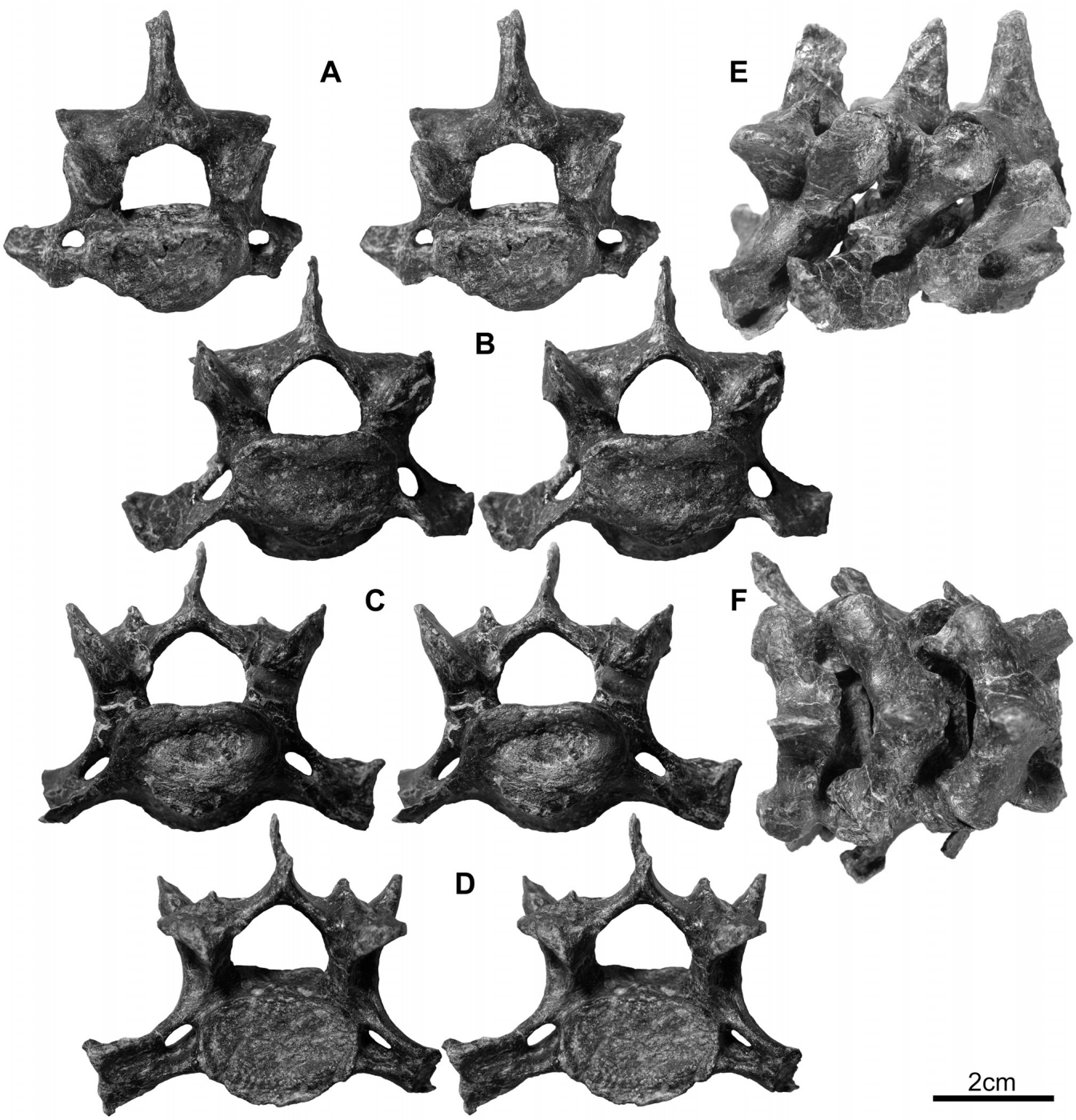

FIGURE 18. Referred fifth, sixth, and seventh cervical vertebrae of *Trogosus castoridens* (SDSNH 40819). **A**–**C**, anterior views (stereograph) of fifth, sixth, and seventh vertebrae; **D**, posterior view (stereograph) of seventh vertebra; **E, F**, articulated cervical vertebrae, right lateral and dorsal views. Anterior at right in lateral and dorsal views (**E, F**).

exhaustive search algorithm were used to examine the resulting tree topologies. In addition, Bremer decay values (Bremer, 1988) and bootstrap values (10,000 bootstrap replicates, values greater than 50% are provided) were computed for each node.

To test the hypothesis that SDSNH 40819 represents a specimen of *T. castoridens*, we combined the character coding of SDSNH 40819 with that of ANSP 10337 to represent a single OTU and then conducted an exhaustive search for all possible tree topologies. All character changes at each node under ACCTRAN and DELTRAN character-state optimization options are reported in Appendix S3 of Supplementary Data.

Results and Discussion

In the analysis using only dental and dentary characters (characters 1–32) to test the hypothesis that SDSNH 40819

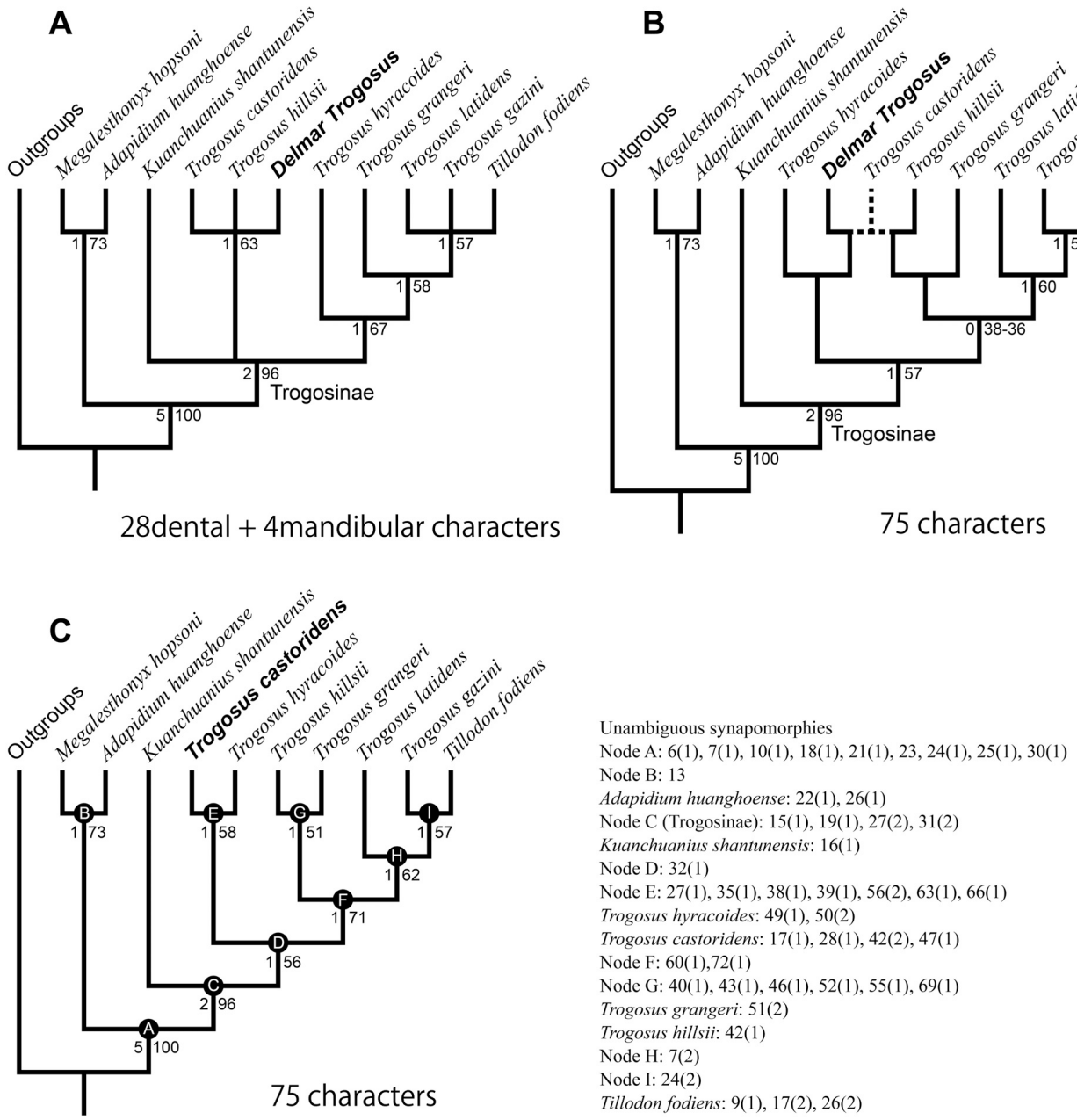

Unambiguous synapomorphies
Node A: 6(1), 7(1), 10(1), 18(1), 21(1), 23, 24(1), 25(1), 30(1)
Node B: 13
Adapidium huanghoense: 22(1), 26(1)
Node C (Trogosinae): 15(1), 19(1), 27(2), 31(2)
Kuanchuanius shantunensis: 16(1)
Node D: 32(1)
Node E: 27(1), 35(1), 38(1), 39(1), 56(2), 63(1), 66(1)
Trogosus hyracoides: 49(1), 50(2)
Trogosus castoridens: 17(1), 28(1), 42(2), 47(1)
Node F: 60(1),72(1)
Node G: 40(1), 43(1), 46(1), 52(1), 55(1), 69(1)
Trogosus grangeri: 51(2)
Trogosus hillsii: 42(1)
Node H: 7(2)
Node I: 24(2)
Tillodon fodiens: 9(1), 17(2), 26(2)

FIGURE 19. Most parsimonious trees generated by PAUP analysis discussed in the text. **A, B**, assumes that SDSNH 40819 is not assignable to *Trogosus castoridens* (character states of SDSNH 40819 are separate from those of ANSP 10337); **C**, assumes that SDSNH 40819 is assignable to *T. castoridens* (combines character states of SDSNH 40819 and ANSP 10337). **A**, strict consensus of the 12 most parsimonious trees based only on dental and mandibular characters (32 characters, see text); **B**, two most parsimonious trees based on all characters, showing different position of *T. castoridens* represented only by ANSP 10337; **C**, single parsimonious tree generated using an exhaustive search for all possible tree topologies, with distribution of unambiguous character states at each node (nodes A–I) (character distribution for outgroups is omitted).

belongs to a new species, a heuristic search recovered 12 equally parsimonious trees with a length of 46 steps, consistency index (CI) of 0.9130, retention index (RI) of 0.9167, and rescaled consistency index (RC) of 0.8370. The strict consensus tree (Fig. 19A) shows the ambiguous position of *Kuanchuanius shantunensis* within the trogosine clade and two weakly supported, unresolved clades: *Trogosus latidens* + *T. gazini* + *Tillodon fodiens* and *T. castoridens* + *T. hillsii* + the Delmar *Trogosus* (SDSNH 40819) (short-faced species clade, hereafter). The monophyly of Trogosinae is well supported with a bootstrap value of 96. However, *Trogosus* is found to be paraphyletic because of the placement of *Tillodon fodiens* as sister to *T. latidens* and *T. gazini* to the exclusion of other trogosine taxa. Importantly, the consensus tree does not falsify the hypothesis that SDSNH 40819 and *T. castoridens* are conspecific. The consensus tree does not differ substantially from the tree topology of Miyata (2007b), except for the equivocal position of *K. shantunensis*. Both

trees recovered a short-faced species clade (*T. castoridens* + *T. hillsiii*). The inclusion of SDSNH 40819 in this clade is weakly supported by a single unambiguous synapomorphy (character 20[1], short i2–p3 distance) in the present study.

In the analysis using all characters (characters 1–75) to test the hypothesis that SDSNH 40819 belongs to a new species, a heuristic search recovered two equally parsimonious trees (112 steps, CI = 0.8571, RI = 0.7895, RC = 0.6767). The two trees agree with each other except for the position of *T. castoridens* (represented only by ANSP 10337), which is positioned as either sister to SDSNH 40819 or to *T. hillsii* (Fig. 19B). The former tree topology does not falsify the hypothesis that SDSNH 40819 and *T. castoridens* are conspecific, whereas the latter does falsify it. Neither tree topology supports existence of the short-faced species clade seen in Figure 19A, and suggest instead that the short-faced trait evolved independently in two lineages. The large amount of missing cranial data (especially for ANSP 10337) is likely responsible for the poor bootstrap support (less than 39) for internal nodes, with the exception of the *T. latidens* + *T. gazini* + *Tillodon fodiens* clade. These results do not unequivocally resolve the phylogenetic relationships of *Trogosus* and reveal weak character support for diagnosis of *T. castoridens*.

In the analysis using all characters and combining SDSNH 40819 and ANSP 10337 as a single OTU (= *T. castoridens*), an exhaustive search recovered a single most parsimonious tree with the same tree length as the tree in Figure 19B (112 steps, CI = 0.8571, RI = 0.7838, RC = 0.6718). The resulting, fully resolved tree (Fig. 19C) recovered a monophyletic Trogosinae (node C), two successive monophyletic species pairs (node E: *T. castoridens* + *T. hyracoides* and node G: *T. grangeri* + *T. hillsii*), and a clade consisting of *T. latidens* + *T. gazini* + *Tillodon fodiens* (node H). Nodes E and G are, respectively, supported by seven (27[1], 35[1], 38[1], 39[1], 56[2], 63[1], 66[1]) and six (40[1], 43[1], 46[1], 52[1], 55[1], 69[1]) unambiguous synapomorphies. These results failed to recognize a monophyletic short-faced species group and instead suggest that the short-faced condition evolved at least twice in trogosine tillodonts. Thus, character 20 (reflecting differences in rostral length) should be viewed as homoplastic.

When Gazin (1953) originally described *T. grangeri* and *T. hillsii* from the Huerfano Formation, Huerfano Basin, Colorado, he noted that this species pair represented two distinct skull types, one long-faced (*T. grangeri*) and one short-faced (*T. hillsii*). Gazin (1953) also noted a similar species pair pattern for trogosines from the Blacks Fork Member of the Bridger Formation, Green River Basin, Wyoming, where *T. hyracoides* (long-faced) and *T. castoridens* (short-faced) occur in the same strata of the same sedimentary basin. In attempting to explain this pattern, Gazin (1953) suggested that these pairs may be due to sexual dimorphism, ontogenetic variation, or taxonomy (i.e., phylogeny). Gazin (1953) emphasized that because of small sample size, it was not possible to rigorously test these three hypotheses, and in the end he opted for a taxonomic explanation with two separate sympatric species from each Eocene sedimentary basin. Robinson (1966) examined additional dental materials of *Trogosus* from the Huerfano Formation and in addressing this question of sexual dimorphism, ontogenetic variation, and taxonomy suggested that individual variation within a single species (= *T. grangeri*) was the most likely explanation. However, Miyata (2007a) suggested that large individuals from the Huerfano Formation should be viewed as *T. latidens*, and no additional material supporting sexual dimorphism is known from the formation (Miyata, 2007a, 2007b). Although Lucas and Schoch (1998) did not specifically discuss the question of North American trogosine dimorphism versus taxonomy, these authors supported the dimorphic hypothesis.

In interpreting the results of the present analysis (Fig. 19C), we found greater support for the original taxonomic hypothesis of Gazin (1953) and thus continue to recognize two sets of sympatric trogosine species pairs: *T. hyracoides* and *T. castoridens* from the Green River Basin (plus San Diego Basin) and *T. hillsii* and *T. grangeri* from the Huerfano Basin. Besides character 20 (short [1] vs. moderate [0] and long [2] i2–p3 or I2–P2 distances), character support for this interpretation of sympatric species pairs includes (in the following listing the former state is shared by short-faced taxa, *T. castoridens* and *T. hillsii*, whereas the latter state is shared by long-faced taxa, *T. hyracoides* and *T. grangeri*): character 11, M3 smaller (0) vs. larger (1) than M2; character 29, moderate (1) vs. deep (2) dentary depth; character 45, weak (0) vs. distinct (1) lateral constriction of rostrum between C1 and P2; character 57, blunt (0) vs. distinct (1) postorbital process; character 61, short but shallow (0) vs. deep (1) sagittal crest. In addition, character 36, posterior extension of palatine process of premaxilla to middle of I3 margin (0) vs. posterior to I3 (1) and character 70, shape of occipital shield concave (0) vs. bulging (1), might also be related to taxonomic dimorphism.

Importantly, we also found characters that provide support for distinguishing between the species pair (*T. hillsii* and *T. grangeri*) from the Huerfano Formation: *T. hillsii* has a faint lacrimal tubercle (character 51[1]), whereas *T. grangeri* has a strong lacrimal tubercle (character 51[2]); *T. hillsii* has a moderately bowed zygomatic arch (character 53[1]), whereas *T. grangeri* has a strongly expanded zygomatic arch (character 53[2]); and *T. hillsii* has a zygion posteriorly placed along the anteroposterior length of orbitotemporal fossa (character 54[1]), whereas *T. grangeri* has a zygion anteriorly placed along the anteroposterior length of orbitotemporal fossa (character 54[0]).

As support for recognizing *T. castoridens* as a distinct species, we found cranial characters that differentiated *T. castoridens* from another short-faced species, *T. hillsii*, and other characters that differentiated *T. castoridens* from sympatric *T. hyracoides*. Concerning *T. castoridens* and *T. hillsii* as different short-faced species, we note that *T. castoridens* has a point-like nasal-maxilla contact (character 42[2]), whereas *T. hillsii* has a longer nasal-maxilla contact (character 42[1]) also seen in *T. grangeri* and *T. hyracoides*. This pattern suggests that rostral shortening in the two species may have evolved in a different manner. Concerning *T. hyracoides* and *T. castoridens* as different species, we note that *T. hyracoides* has some unique (possibly autapomorphic) characters of the lacrimal not shared with *T. castoridens*: concave facial process not extending anteriorly beyond the orbital rim (character 49[1]) and lacrimal foramen positioned posterior to orbital rim (character 50[2]). However, we want to caution that there is currently insufficient information to determine whether these lacrimal characters should be viewed as dimorphic features of a single species or as distinctive features of two separate species. As originally emphasized by Gazin (1953), we must wait until additional well-preserved fossils of *T. hyracoides* and *T. castoridens* are discovered and described from the Green River Basin before hoping to clarify the relationships within the *T. hyracoides* + *T. castoridens* species pair.

CONCLUSIONS

The well-preserved fossil remains (SDSNH 40819) of a trogosine tillodont from the Swami's Point local fauna of the Delmar Formation in coastal San Diego County, California, U.S.A., represent the first record of these enigmatic Paleogene mammals from the west coast. Our examination of the recovered remains, which include a nearly complete skull

with a fairly unworn dentition, determined that the Delmar tillodont is conspecific with a short-faced trogosine, *Trogosus castoridens* Leidy, 1871, formerly known only from the holotype (ANSP 10337) from the Blacks Fork Member of the Bridger Formation exposed at the Grizzly Buttes, Green River Basin, Wyoming. The co-occurrence of *T. castoridens* with *Hyrachyus modestus* and the placement within Chron 21r suggest a most likely correlation with Br2.

Incorporation of SDSNH 40819 into an expanded phylogenetic analysis of trogosine tillodonts helps to better resolve phylogenetic relationships within this group. Our findings support the recognition of sympatric species pairs of *Trogosus*, one pair (*T. castoridens* and *T. hyracoides*) in the Eocene Green River Basin and another (*T. hillsii* and *T. grangeri*) in the Eocene Huerfano Basin. Each sympatric pair consists of a short-faced species and a long-faced species. This hypothesized pattern of sympatric species pairs was originally proposed by Gazin (1935), but remains controversial in light of the relatively small sample size and paucity of well-preserved trogosine fossils. The recognition of a short-faced *Trogosus* from the Eocene San Diego Basin poses interesting, but unanswered questions concerning tillodont biogeography near the early-middle Eocene boundary.

ACKNOWLEDGMENTS

We express our gratitude to G. F. Gunnell (Duke University, Duke Lemur Center), K. A. Randall (SDSNH), J. Meng and J. Galkin, (AMNH), T. Daeschler (ANSP), P. D. Gingerich (UM), K. C. Beard (Carnegie Museum of Natural History), and R. J. Emry and N. D. Pyenson (USNM) for giving permission and assistance to examine the specimens under their care. We also greatly thank G. F. Gunnell for providing a cast of *Azygonyx*. We also appreciate the critical comments from the two outside reviewers, Patricia A. Holroyd (Museum of Paleontology, University of California, Berkeley) and G. F. Gunnell, which improved the manuscript.

LITERATURE CITED

Alexander, J. P., and B. J. Burger. 2001. Stratigraphy and taphonomy of Grizzly Buttes, Bridger Formation, and the middle Eocene of Wyoming; pp. 165–196 in G. F. Gunnell (ed.), Eocene Biodiversity: Unusual Occurrences and Rarely Sampled Habitats. Kluwer Academic/Plenum Publishers, New York, New York.

Bottjer, D. J., S. P. Lund, J. E. Powers, M. C. Steele, and R. L. Squires. 1991. Magnetostratigraphy of Paleogene strata in San Diego and the Simi Valley, southern California; pp. 115–123 in P. L. Abbott and J. A. May (eds.), Eocene Geologic History, San Diego Region. SEPM Pacific Section Publication 68, Los Angeles, California.

Bown, T. M., and M. J. Kraus. 1979. Origin of the tribosphenic molar and metatherian and eutherian dental formulae; pp. 172–181 in J. A. Lillegraven, Z. Kielan-Jaworowska, and W. A. Clemens (eds.), Mesozoic Mammals: The First Two-Thirds of Mammalian History. University of California Press, Berkeley, California.

Bremer, K. 1988. The limits of amino acid sequence data in angiosperm phylogenetic reconstruction. Evolution 42:795–803.

Bukry, D., and M. P. Kennedy. 1969. Cretaceous and Eocene coccoliths at San Diego, California. California Division of Mines and Geology Special Report 100:33–43.

Chow, M. 1963. Tillodont materials from Eocene of Shantung and Honan. Vertebrata PalAsiatica 7:97–104. [Chinese 97–100; English 101–104]

Cifelli, R. L. 1982. The petrosal structure of *Hyopsodus* with respect to that of some other ungulates, and its phylogenetic implications. Journal of Paleontology 56:795–805.

Colbert, M. W., and R. M. Schoch. 1998. Tapiroidea and other moropomorphs; pp. 569–582 in C. M. Janis, K. M. Scott, and L. L. Jacobs (eds.), Evolution of Tertiary Mammals of North America, Volume 1: Terrestrial Carnivores, Ungulates, and Ungulatelike Mammals. Cambridge University Press, Cambridge, U.K.

Coombs, M. C., and W. P. Coombs. 1982. Anatomy of the ear region of four Eocene artiodactyls: *Gobiohyus*, ?*Helohyus, Diacodexis* and *Homacodon*. Journal of Vertebrate Paleontology 2:219–236.

Cope, E. D. 1883. On the mutual relations of the bunotherian Mammalia. Proceedings of the Academy of Natural Sciences of Philadelphia 35: 77–83.

Emry, R. J. 1990. Mammals of the Bridgerian (middle Eocene) Elderberry Canyon Local Fauna of eastern Nevada; pp. 187–210 in T. M. Bown and K. D. Rose (eds.), Dawn of the Age of Mammals in the Northern Part of the Rocky Mountain Interior, North America. Geological Society of America Special Paper 243.

Evans, H. E. (ed.). 1993. Miller's Anatomy of the Dog, 3rd revised edition. W. B. Saunders Company, Philadelphia, Pennsylvania, 1113 pp.

Flynn, J. J. 1986. Correlation and geochronology of middle Eocene strata from the western United States. Palaeogeography, Palaeoclimatology, Palaeoecology 55:335–406.

Frederiksen, N. O. 1991. Age determinations for Eocene formations of the San Diego, California area, based on pollen data; pp. 195–199 in P. L. Abbott and J. A. May (eds.), Eocene Geologic History, San Diego Region. SEPM Pacific Section Publication 68, Los Angeles, California.

Gazin, C. L. 1953. The Tillodontia: an early Tertiary order of mammals. Smithsonian Miscellaneous Collections 121(10):1–110.

Gazin, C. L. 1976. Mammalian faunal zones of the Bridger Middle Eocene. Smithsonian Contributions to Paleobiology 26:1–23.

Geisler, J. H., and M. C. McKenna. 2007. A new species of mesonychian mammal from the lower Eocene of Mongolia and its phylogenetic relationships. Acta Palaeontologica Polonica 52:189–212.

Gingerich, P. D., and G. F. Gunnell. 1979. Systematics and evolution of the genus *Esthonyx* (Mammalia, Tillodontia) in the early Eocene of North America. Contributions from the Museum of Paleontology, University of Michigan 25:125–153.

Gunnell, G. F. 1998. Mammalian fauna from the lower Bridger Formation (Bridger A, early middle Eocene) of the southern Green River Basin, Wyoming. Contributions from the Museum of Paleontology, University of Michigan 30:83–130.

Gunnell, G. F., P. C. Murphey, R. K. Stucky, K. E. B. Townsend, P. Robinson, J.-P. Zonneveld, and W. S. Bartels. 2009. Biostratigraphy and biochronology of the latest Wasatchian, Bridgerian, and Uintan North American Land Mammal 'Ages'. Museum of Northern Arizona Bulletin 65:279–330.

International Anatomical Nomenclature Committee. 1983. Nomina Anatomica, 5th edition. Lippincott Williams and Wilkins, Philadelphia, Pennsylvania, 196 pp.

International Committee on Veterinary Gross Anatomical Nomenclature. 2012. Nomina Anatomica Veterinaria, revised version of the 5th edition. Available at www.wava-amav.org/Downloads/nav_2012.pdf. Accessed December 1, 2013.

Kennedy, M. P. 1975. Geology of the San Diego metropolitan area, California: section A, Western San Diego metropolitan area. California Division of Mines and Geology, Bulletin 200:7–39.

Leidy, J. 1870. Remarks on a collection of fossils from the western territories. Proceedings of the Academy of Natural Sciences of Philadelphia 22:109–110.

Leidy, J. 1871. Remains of extinct mammals from Wyoming. Proceedings of the Academy of Natural Sciences of Philadelphia 23:113–116.

Lucas, S. G., and R. M. Schoch. 1998. Tillodontia; pp. 268–273 in C. M. Janis, K. M. Scott, and L. L. Jacobs (eds.), Evolution of Tertiary Mammals of North America, Volume 1: Terrestrial Carnivores, Ungulates, and Ungulatelike Mammals. Cambridge University Press, Cambridge, U.K.

Marsh, O. C. 1871. Notice of some new fossil mammals from the Tertiary Formation. American Journal of Science and Arts 2:35–44.

Marsh, O. C. 1873. Notice of new Tertiary mammals. (continued). American Journal of Science and Arts 5:485–488.

Marsh, O. C. 1874. Notice of new Tertiary mammals. III. American Journal of Science and Arts 7:531–534.

Marsh, O. C. 1875. New order of Eocene mammals. American Journal of Science and Arts 9:221.

May, J. A., and J. E. Warme. 1991. Marine sedimentology of the early to middle Eocene La Jolla Group; pp. 73–88 in P. L. Abbott and J. A. May (eds.), Eocene Geologic History, San Diego Region. SEPM Pacific Section Publication 68, Los Angeles, California.

May, J. A., J. M. Lohmar, J. E. Warme, and S. Morgan. 1991. Field trip guide: early to middle Eocene La Jolla Group of Black's Beach, La Jolla, California; pp. 27–36 in P. L. Abbott and J. A. May (eds.), Eocene Geologic History, San Diego Region. SEPM Pacific Section Publication 68, Los Angeles, California.

Miyata, K. 2007a. New material of Asian *Trogosus* (Tillodontia, Mammalia) from the Akasaki Formation, Kumamoto Prefecture, Japan. Journal of Vertebrate Paleontology 27:176–188.

Miyata, K. 2007b. New species of *Trogosus* (Tillodontia, Mammalia) from the Green River Basin, Wyoming, U.S.A. Journal of Vertebrate Paleontology 27:661–675.

Miyata, K., and Y. Tomida. 1998. *Trogosus*-like tillodont (Tillodontia, Mammalia) from the early middle Eocene of Japan. Paleontological Research 2:193–198.

Moore, E. J. 1987. Tertiary marine pelecypods of California and Baja California: Plicatulidae to Ostreidae. U.S. Geological Survey Professional Paper 1228C:1–53.

Novacek, M. J. 1986. The skull of leptictid insectivorans and the higher-level classification of eutherian mammals. Bulletin of the American Museum of Natural History 183:1–112.

Novacek, M. J. 1993. Patterns of diversity in the mammalian skull; pp. 438–545 in J. Hanken and B. K. Hall (eds.), The Skull. Volume 2: Patterns of Structural Systematic Diversity. University of Chicago Press, Chicago, Illinois.

Radinsky, L. B. 1966. The families of the Rhinocerotoidea. Journal of Mammalogy 47:631–639.

Radinsky, L. B. 1967. *Hyrachyus, Chasmotherium*, and the early evolution of helaletid tapiroids. American Museum Novitates 2313:1–23.

Robinson, P. 1966. Fossil Mammalia of the Huerfano Formation, Eocene, of Colorado. Peabody Museum of Natural History, Yale University, Bulletin 21:1–95.

Robinson, P., G. F. Gunnell, S. L. Walsh, W. C. Clyde, J. E. Storer, R. K. Stucky, D. J. Froehlich, I. Ferrusquia-Villafranca, and M. C. McKenna. 2004. Wasatchian through Duchesnean biochronology; pp. 106–155 in M. O. Woodburne (ed.), Late Cretaceous and Cenozoic Mammals of North America: Biostratigraphy and Geochronology. Columbia University Press, New York, New York.

Schoch, R. M. 1984. Two unusual specimens of *Helaletes* in the Yale Peabody Museum collections, and some comments on the ancestry of the Tapiridae (Perissodactyla, Mammalia). Postilla 193:1–20.

Smith, K. T., and P. A. Holroyd. 2003. Rare taxa, biostratigraphy, and the Wasatchian-Bridgerian boundary in North America; pp. 501–511 in S. L. Wing, P. D. Gingerich, B. Schmitz, and E. Thomas (eds.), Causes and Consequences of Globally Warm Climates in the Early Paleogene. Geological Society of America Special Paper 369.

Smith, M. E., A. R. Carroll, and B. S. Singer. 2008. Synoptic reconstruction of a major ancient lake system: Eocene Green River Formation, western United States. Geological Society of America Bulletin 120:54–84.

Smith, M. E., K. R. Chamberlain, B. S. Singer, and A. R. Carroll. 2010. Eocene clocks agree: coeval $^{40}Ar/^{39}Ar$, U–Pb, and astronomical ages from the Green River Formation. Geology 38: 527–530.

Stucky, R. K., and L. Krishtalka. 1983. Revision of the Wind River faunas, early Eocene of central Wyoming. Part 4. The Tillodontia. Annals of Carnegie Museum 52:375–391.

Swofford, D. L. 2003. PAUP* 4.0: Phylogenetic Analysis Using Parsimony (*And Other Methods), version 4.0b10. Sinauer Associates, Sunderland, Massachusetts.

Tsukui, K., and W. C. Clyde. 2012. Fine-tuning the calibration of the early to middle Eocene geomagnetic polarity time scale: paleomagnetism of radioisotopically dated tuffs from Laramide foreland basins. Geological Society of America Bulletin 124: 870–885.

Vandenberghe, N., F. J. Hilgen, and R. P. Speijer. 2012. The Paleogene Period; pp. 855–921 in F. M. Gradstein, J. G. Ogg, M. D. Schmitz, and G. M. Ogg (eds.), The Geologic Time Scale 2012, Volume 2. Elsevier BV, Oxford, U.K.

Walsh, S. L. 1996. Middle Eocene mammal faunas of San Diego County, California; pp. 75–119 in D. R. Prothero and R. J. Emry (eds.), The Terrestrial Eocene-Oligocene Transition in North America. Cambridge University Press, New York, New York.

Wang, Y., and X. Jin. 2004. A new Paleocene tillodont (Tillodontia, Mammalia) from Qianshan, Anhui, with a review of Paleocene tillodonts from China. Vertebrata PalAsiatica 42:13–26.

Warme, J. E. 1991. Delmar Formation and Torrey Sandstone as exposed along beach cliffs, Solana Beach, northern San Diego County; pp. 39–54 in P. L. Abbott and J. A. May (eds.), Eocene Geologic History, San Diego Region. SEPM Pacific Section Publication 68, Los Angeles, California.

Wible, J. R. 2003. On the cranial osteology of the short-tailed opossum *Monodelphis brevicaudata* (Didelphidae, Marsupialia). Annals of Carnegie Museum 72:137–202.

Wible, J. R. 2008. On the cranial osteology of the Hispaniolan solenodon, *Solenodon paradoxus* Brandt, 1833 (Mammalia, Lipotyphla, Solenodontidae). Annals of Carnegie Museum 77:321–402.

Wible, J. R. 2011. On the treeshew skull (Mammalia, Placentalia, Scandentia). Annals of Carnegie Museum 79:149–230.

Wood, H. E. 1934. Revision of the Hyrachyidae. Bulletion of the American Museum of Natural History 67:181–295.

Woodburne, M. O. 2004. Global events and the North American mammalian biochronology; pp. 315–343 in M. O. Woodburne (ed.), Late Cretaceous and Cenozoic Mammals of North America: Biostratigraphy and Geochronology. Columbia University Press, New York, New York.

Submitted January 29, 2015; revisions received May 9, 2015;
accepted August 29, 2015.
Handling editor: Edward Davis.